

AD-753 366

BUCKLING OF CYLINDRICAL SHELLS SUBJECTED
TO AXIAL LOADING

Louis R. Fuka

Texas University

Prepared for:

Army Natick Laboratories

September 1971

DISTRIBUTED BY:

NTIS

National Technical Information Service
U. S. DEPARTMENT OF COMMERCE
5285 Port Royal Road, Springfield Va. 22151

753366

AD

Technical Report

72-50-AD

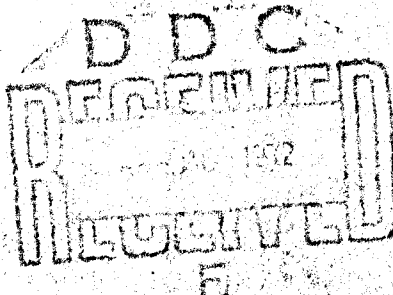
BUCKLING OF CYLINDRICAL SHELLS SUBJECTED TO AXIAL LOADING

by

Louis R. Fuka

The University of Texas at Austin

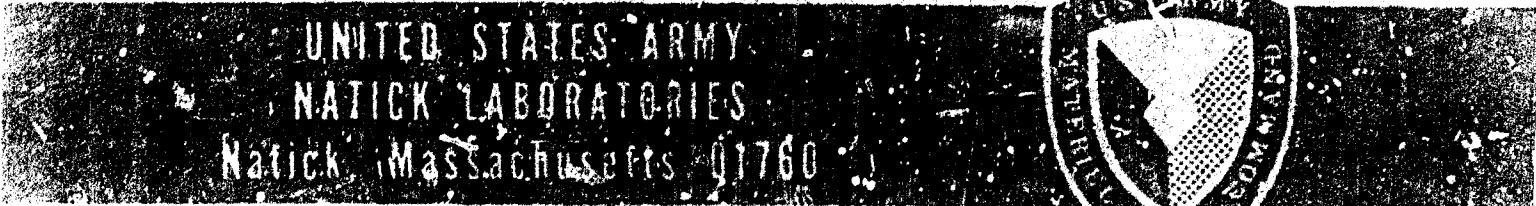
Austin, Texas



Contract No. DAAG 17-70-C-0127

Approved for public release; distribution unlimited.

September 1971



NATIONAL TECHNICAL INFORMATION SERVICE

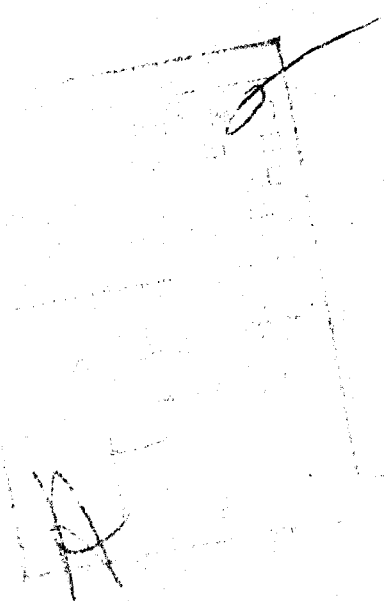
Airdrop Engineering Laboratory

Best Available Copy

Approved for public release; distribution unlimited.

Citation of trade names in this report does not constitute an official indorsement or approval of the use of such items.

Destroy this report when no longer needed. Do not return it to the originator.



Approved for Public Release;
Distribution Unlimited.

AD _____

TECHNICAL REPORT

72-50-AD

Buckling of Cylindrical Shells
Subjected to Axial Loading

by

Louis R. Fuka

Engineering Mechanics Research Laboratory
The University of Texas at Austin
Austin, Texas

Contract No. DAAG17-70-C-0127

Project Reference
1F1 62203 D195

September 1971

-id-

Airdrop Engineering Laboratory
U. S. Army Natick Laboratories
Natick, Massachusetts 01760

FOREWORD

This work was performed under US Army Natick Laboratories Contract No. DAAG17-70-C-0127 during the period of 1 Apr 70 to 31 Mar 71. The Project No. was 1F162203D195 entitled "Exploratory Development of Airdrop Systems", and the Task was No. 13 entitled "Impact Phenomena". Messrs. Edward J. Giebutowski and Marshall S. Gustin of the Airdrop Engineering Laboratory served as the Project Officers.

The effort is part of a continuing investigation directed toward obtaining a better understanding of the failure mechanism of energy dissipater materials, and the response of airdroppable supplies and equipment to airdrop impact phenomena; and toward obtaining improved airdrop energy dissipater materials and techniques.

This report is concerned primarily with an analytical study of the configuration change of an individual cell of paper honeycomb energy dissipater material as it is crushed, in order to determine the relative effect of changes in various cell design characteristics on level of strength and uniformity of performance.

Security Classification

DOCUMENT CONTROL DATA - R & D

(Security classification of title, body of abstract and indexing annotation must be entered when the overall report is classified)

1. ORIGINATING ACTIVITY (Corporate author) Engineering Mechanics Research Laboratory The University of Texas at Austin Austin, Texas 78712		2a. REFERENCE SECURITY CLASSIFICATION	
		2b. GROUP	
3. REPORT TITLE BUCKLING OF CYLINDRICAL SHELLS SUBJECTED TO AXIAL LOADING			
4. DESCRIPTIVE NOTES (Type of report and inclusive dates) Annual Report 1 Apr 70 - 31 Mar 71			
5. AUTHOR(S) (First name, middle initial, last name) Louis R. Fuka			
6. REPORT DATE September 1971		7a. TOTAL NO. OF PAGES 88 78	7b. NO. OF REFS 14
8a. CONTRACT OR GRANT NO. Contract No. DAAG17-70-G-0127		9a. ORIGINATOR'S REPORT NUMBER(S) EMRL 1091	
b. PROJECT NO. 1F162203DL95		9b. OTHER REPORT NO(S) (Any other numbers that may be assigned this report) 72-50-AD	
c. Task No. 13		d.	
10. DISTRIBUTION STATEMENT Approved for public release; distribution unlimited. Details of illustrations in this document may be better studied on microfiche.			
11. SUPPLEMENTARY NOTES		12. SPONSORING MILITARY ACTIVITY Airdrop Engineering Laboratory US Army Natick Laboratories Natick, Mass 01760	
13. ABSTRACT Mathematically exact equations of the deflections required for a circular cylinder to buckle into a developable polyhedral shape are derived. From this equation it is seen that the tangential displacement can be readily related to the radial displacement. The exact formulas for coefficients of a Fourier series representing the radial displacements are derived for a buckled circular cylinder having any longitudinal and circumferential mode numbers. This is in contrast to earlier work in which approximate Fourier coefficients were derived for large values of circumferential mode number ($n \geq 10$). The analytical expressions are derived to study buckling of individual hexagonal cells in paper honeycomb. The honeycomb cells are originally in the developable shape represented by the circumferential mode number $n=6$ and longitudinal mode number $m=0$. With the guidance of the analytical expressions described above, it has been observed that individual honeycomb cells constrained by surrounding honeycomb cells in an impacted honeycomb pad, buckle in a modified form of the $n=3$ deflection shape. This modified deflection shape is determined as a function of the width of the glue line joining the cells which remain intact after crushing, that is the effective glue line width. The analytical expressions of the Fourier coefficients of the radial displacements of the modified $n=3$ deflection shape are derived. The net radial displacements of the impacted buckled hexagonal shell are obtained by subtracting the Fourier series representing the original hexagonal cylindrical shape corresponding to the $n=6, m=0$ mode from the Fourier series representing the modified $n=3$ buckling shape. This net deflection is inserted in the strain energy equations to obtain (continued)			

DD FORM 1473
1 NOV 66

REPLACES DD FORM 1473, 1 JAN 64, WHICH IS OBSOLETE FOR ARMY USE.

- 10 -

Security Classification

14 KEY WORDS	LINK A		LINK B		LINK C	
	ROLE	WT	ROLE	WT	ROLE	WT
Buckling	8		4			
Deformation	8		4			
Cylindrical Shells	1, 7		-		4, 7	
Cylinders	1, 7		9		4, 7	
Paper Honeycomb	4					
Impact Shock	6					
Statistics			8			
Longitudinal			0			
Circumferential			0			
Fourier Series			10			
Stress Analysis					8	
Strain Energy Methods					10	
Equations					10	
Hexagonal Shells	2				4	
Radius/Thickness					6	
Radius/Length					6	
Glue Line Width					6	
Poisson's Ratio					6	
Young's Modulus					6	
Parameters					6	
Geometric					0	

- 1b

TABLE OF CONTENTS

	Page
FOREWORD	ii
TABLE OF CONTENTS	iii
LIST OF FIGURES	iv
ABSTRACT	v
INTRODUCTION	1
1. Background	1
2. Previous Work	4
3. Present Investigation	6
PROCEDURE	7
1. Developable Surface Deflection Shape .	8
2. Honeycomb Deflection Shapes	10
3. Buckling Stress	17
RESULTS	18
1. Developable Polyhedral Surface Equations	18
2. Computer Check	21
3. Honeycomb Cell Shape Equations	21
4. Buckling Stress	24
CONCLUSIONS AND RECOMMENDATIONS	30
REFERENCES	31
LIST OF SYMBOLS	32
APPENDIX	35
Derivation of Equations	35
1. Exact Displacements	35
2. Fourier Series Expansion in θ	44
3. Determination of Fourier Coefficients for Double Fourier Series	50
4. Fourier Coefficient for Honeycomb Cell	53
5. Strain Energy Expressions	59

LIST OF FIGURES

Figure		Page
1.	Paper Honeycomb Pad	2
2.	Ideal Inextensional and Actual Collapse Patterns	3
3.	Transformation of a Cylinder into a Polyhedral Surface	5
4.	Axial Cross Sections	9
5.	Initial Circular Cylinder and Hexagonal Cylinder	11
6.	Honeycomb Cell Displacement Pattern After Crushing	12
7.	Profile of Circular Cylinder Buckling in $n=6$, $m=0$, and $n=3$ Modes	14
8.	Profile of Circular Cylinder Buckled in $n=6$, $m=0$; $n=3$ and Modified $n=3$ Modes ..	15
9.	Radial Displacement at $\theta=0$ for Different Values of I	22
10.	Buckling Stress Variation with Cell Thickness	25
11.	Buckling Stress Variation with Glue Line Width	27
12.	Buckling Stress Variation with Poisson's Ratio	29
A 1	Cross Sections of Deformed Cylinder Between Axial Nodes	37
A 2a	Detailed Cross Sections of Deformed Cylinder Between Axial Nodes	38
A 2b	Detailed Cross Sections of Deformed Cylinder Between Axial Nodes	39
A 3	Detailed Portion of Cross Section Used for Determination of Radial and Tangential Displacements	41
A 4	Detailed Axial Section for u Displacement Determination	45
A 5	Modified Form of $n=3$ Mode Shape	54
A 6	End Condition Effects on Mode Shape ...	55

ABSTRACT (Continued)

the total elastic strain energy, bending and stretching strain energies, and buckling stress. These quantities are obtained for hexagonal shells with variations in various geometrical parameters, such as radius/thickness, radius/length, effective glue line width and the mechanical properties; Poisson's ratio and Young's modulus.

ABSTRACT

To obtain some insight into the failure mechanism of paper honeycomb and to identify the significant parameters an analysis has been made of the buckling of a thin walled, axially loaded cylinder with a hexagonal cross section. The analysis begins with a derivation of mathematically exact expressions for the radial deflections required to change a circularly cylindrical shell into a developable polyhedral shape. This expression is then put into the form of a Fourier series which represents the radial displacements of a buckled circular cylindrical shell having any longitudinal and circumferential mode numbers. Hexagonal honeycomb cells have the developable shape given by that Fourier series for the circumferential mode $n = 6$ and the longitudinal mode $m = 0$. From this analytical expression it is observed that individual honeycomb cells in an impact loaded honeycomb pad buckle in a modified form of the $n = 3$ deflection shape. This modified shape is determined as a function of the width of the glue line joining the cells. This is referred to as the effective glue line width.

The net radial displacements of the impact buckled hexagonal cell are obtained by subtracting the Fourier series representing the original hexagonal cylindrical shape corresponding to the $n = 6, m = 0$ mode from the Fourier series for the modified $n = 3$ buckling shape. This net deflection is inserted in the strain energy expressions for the total elastic strain energy, including both bending and stretching strains. Using these energy expressions the buckling stress is computed.

Buckling stresses are determined for hexagonal cells in which variations in the geometrical parameters, radius/thickness, radius/length, and effective glue line width are introduced. In addition the mechanical properties, Poisson's ratio and Young's modulus are varied.

The effective glue line width is shown to be the most significant parameter.

INTRODUCTION

1. Background

Paper honeycomb, shown in Fig. 1, has been used for the past 15 years as an energy dissipation device for cushioning supplies and equipment airdropped by parachute. Its outstanding advantages are low cost, lightweight, and a crushing strength that is essentially independent of variations in parameters such as impact velocity and moisture content.

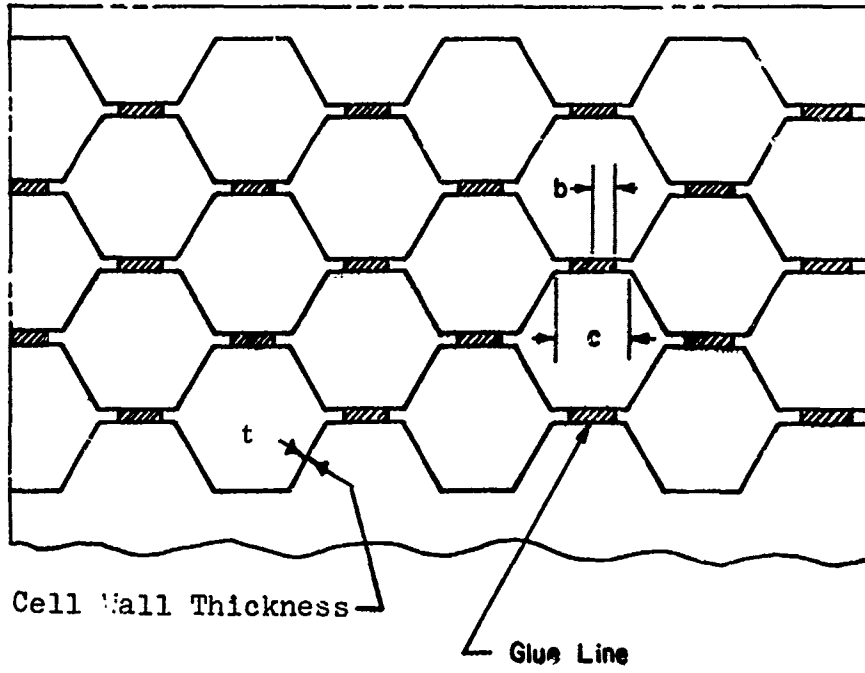
The configuration of the honeycomb pads presently used for impact cushioning was chosen on an empirical basis, because, unfortunately, the critical parameters in the energy dissipating process have not yet been identified. It is known that the crushing stress increases with the honeycomb density, but how the cell size, paper weight, and glue line width individually affect the crushing stress has not been determined. One of the particularly puzzling aspects of the behavior of paper honeycomb has been the variation observed in the crushing strength of apparently identical honeycomb pad specimens.

The purpose of this investigation is to study analytically, the effects of cell size, wall thickness, and glue line width on the crushing load of a honeycomb pad. The primary objective of the study has been the development of a rational guide for the design and construction of honeycomb pads for various specific applications. It was also intended that the analysis would lead to energy dissipation configurations superior to those of honeycomb presently in use.

The approach taken in this investigation is primarily analytical, guided by limited experimentation. An analytical rather than experimental approach was taken because of the difficulty in obtaining consistent test results even with specimens produced by a rigidly controlled fabrication process in which no parameter variations are included.

In order to achieve this, finite deflection buckling of a single cell is analyzed as though the stresses stay within the elastic range during the entire buckling process. Actually it is not unreasonable to assume elastic buckling. Plastic deformation has to occur for significant energy dissipation, but it occurs for the most part after the initial buckling has occurred.

The buckle pattern of cells in honeycomb pads crushed statically or dynamically resembles the buckle pattern of circular cylindrical shells subjected to axial impact as shown in Fig. 2b. In the original approach to this problem it was intended that critical parameters would be determined by representing the honeycomb cells, which initially have



CROSS SECTION

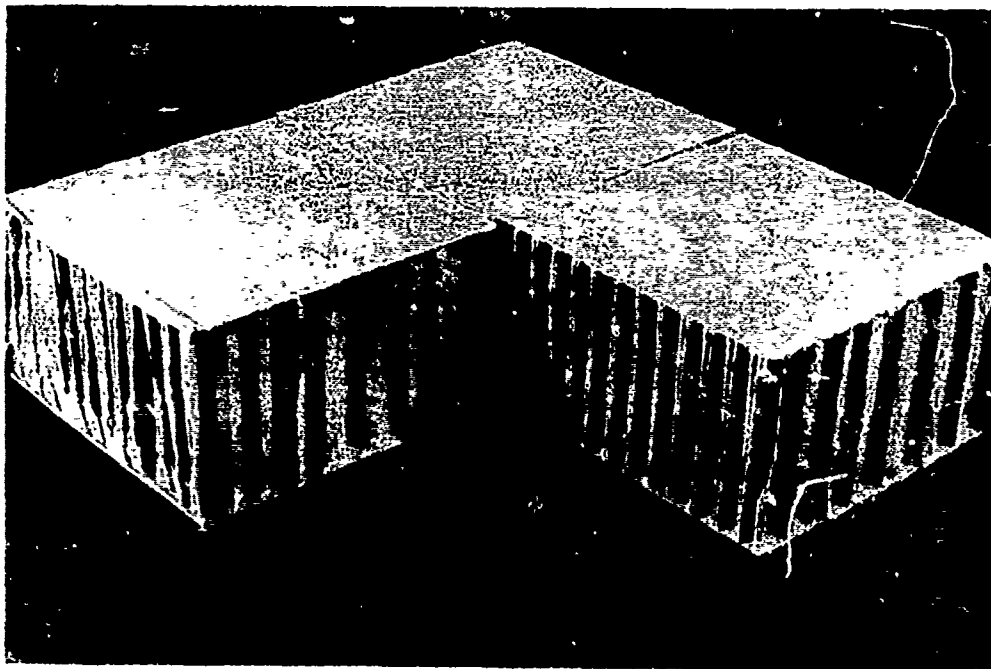


Fig. 1 Paper Honeycomb Pad

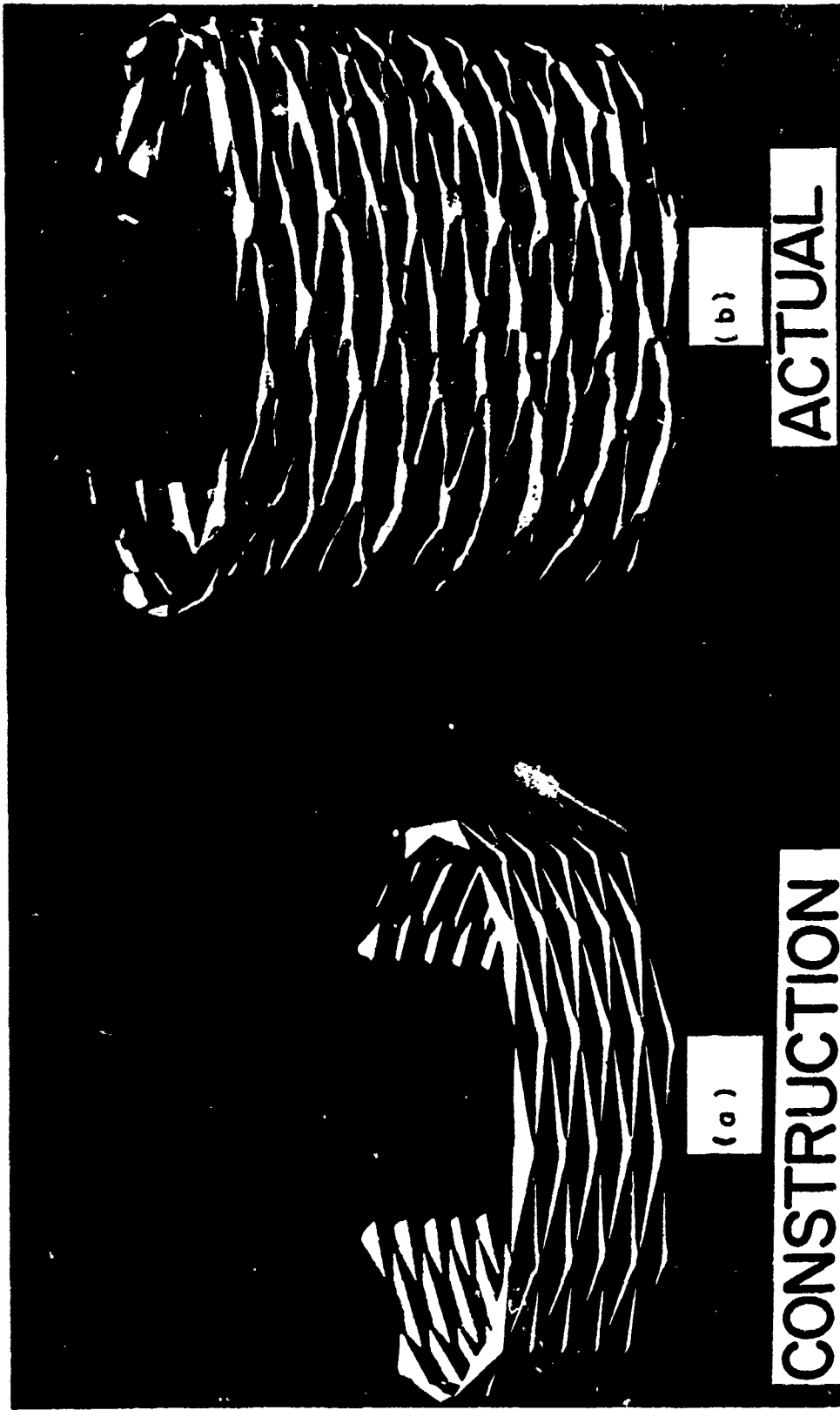


Fig. 2 Ideal Inextensional and Actual Collapse Patterns. (From Cuppa)



Microfilm Edition of this document is available from the University Microfilms International, 300 North Zeeb Road, Ann Arbor, Michigan 48106, U.S.A.

rounded hexagonal cross section shapes, as circular cylindrical shells subjected to impact loading. The discovery of a Fourier series expansion for the developable surfaces made it possible to investigate the behavior of a hexagonal cell.

2. Previous Work

Much of the most significant analytical and experimental work concerning longitudinal impact loading of thin circular, cylindrical and conical shells has been done by Coppa.^{1,2,3} He found that the buckled shape of impacted cylindrical shells is similar to the developable polyhedral shape qualitatively described by Yoshimura and shown in Fig. 3.

a. Shell Impact

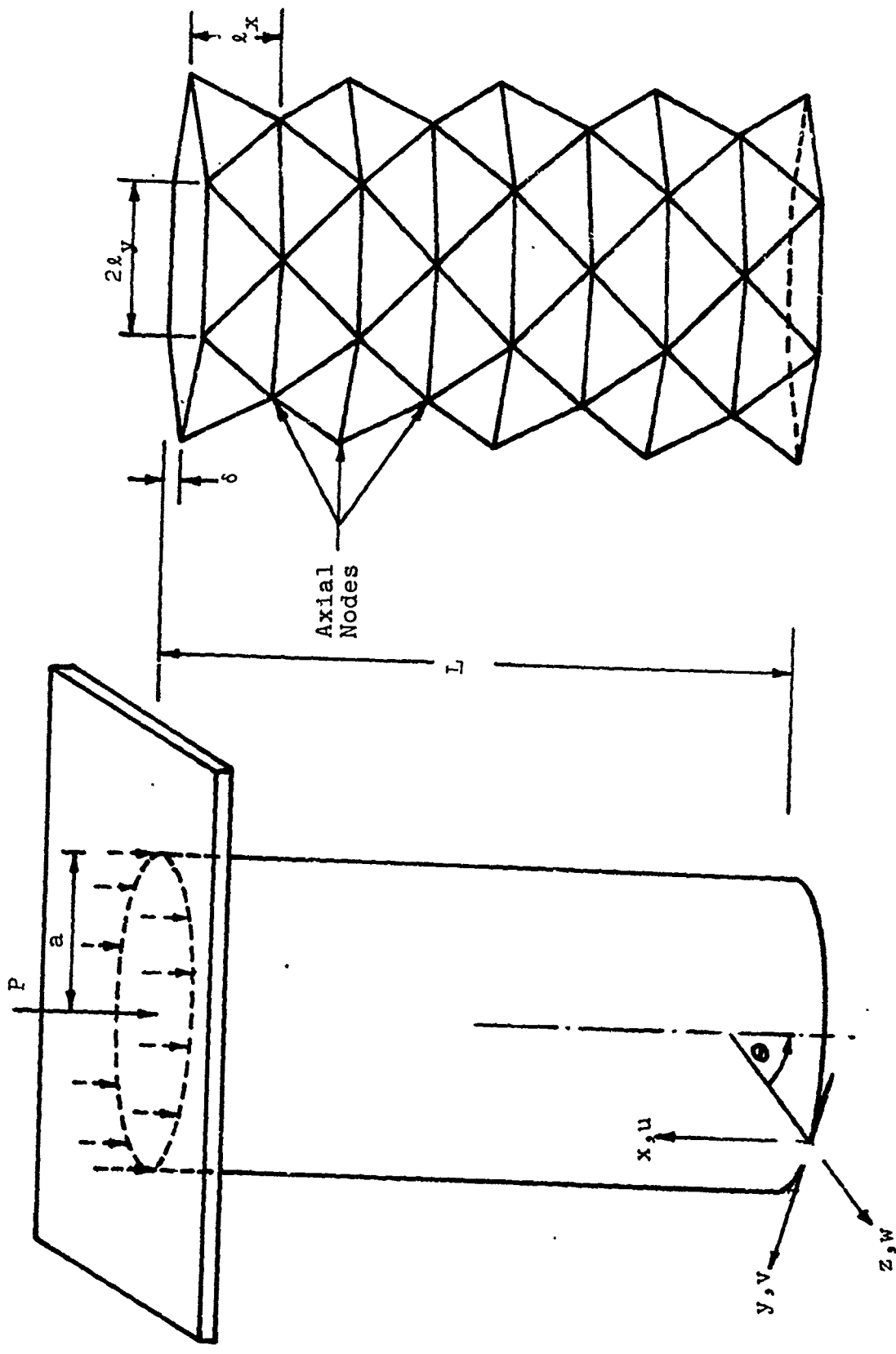
Coppa suggested that buckling of cylindrical and conical shells subjected to longitudinal impact is a phenomenon related to the propagation of stress waves generated at the impacted end of the shell.

The induced stress wave propagates through the length of the shell until it exceeds the critical buckling stress of a section of the shell length. If the initial stress produced at the impacted end is not large enough to exceed the critical buckling stress, the initial stress amplitude is successively increased by reflection at the ends of the shell during stress wave propagation until a critical local buckling stress is reached and local buckling commences. This stress increase phenomenon is produced during stress wave propagation by reflection from the higher acoustic impedance boundaries at the shell ends. The acoustic impedance is defined as the product of the square root of the elastic modulus and the mass density of a material. Coppa's hypothesis is corroborated to some extent by the experimental observation that in his cylinders and in University of Texas honeycomb test specimens, the buckles tend to occur first at the top and bottom of the shell or cell walls. Honeycomb cells appear to buckle at midlength only after very extensive crushing. This characteristic may be due to the buckle inhibiting effect of entrapped air.

b. Developable Polyhedral Surface

Yoshimura pointed out that it is possible for a cylindrical surface to buckle into a developable polyhedral shape as shown in Fig. 3b. This developable polyhedral shape is composed of a number of plane surface panels which have no extensional strain. There is infinite curvature at the sharp fold edges. Yoshimura suggested that the exact deflections for this developable surface might be represented by a Fourier series with an infinite number of terms.

Furthermore, Yoshimura suggested that the deflections of buckled, finite thickness, cylinders with the small radii



(a) Initial Cylinder

(b) Buckled Polyhedral Surface
 $n = 6$ $m = 8$

Fig. 3 Transformation of a Cylinder into a Polyhedral Surface

of curvatures that occur at the rounded fold edges as shown in Fig. 2b, could be approximated by a truncated form of the infinite Fourier series. Yoshimura used only a few terms in his Fourier series representation of the displacements required for the developable surface and described the surface more in qualitative than in quantitative terms.

Hoff, Madsen and Mayer⁵ derived an approximate formula for the coefficients of a Fourier series representing the deflections of a cylindrical surface deformed into a polyhedral surface. This formula is apparently valid for values of the circumferential mode number n equal to or greater than 10. Yoshimura's hypothesis of the developable shape was verified by comparing the values of the coefficients of a Fourier series for describing the buckled shape of very thin axially loaded cylinders. It was found that the larger the number of terms used in the series, the closer the shape approached the developable shape qualitatively described by Yoshimura.

3. Present Investigation

A few static and impact tests were performed on shells in order to observe the buckling patterns and crushing strengths under both types of loading. Observation of the buckle patterns was helpful in the derivation of formulas for the displacements required to produce developable surfaces.

The equations for the exact radial displacements required for a circular cylindrical surface to deform into a developable polyhedral surface are derived from geometrical considerations. A formula for the coefficients of a Fourier series expansion for the exact radial displacements valid for all values of n is then derived. A simple relation which exists between the radial and tangential displacements eliminates the necessity of determining Fourier coefficients for the tangential displacement. It is shown that the initial hexagonal cross section can be expressed in a Fourier series representation, which provides a better model than the circular cross section shell initially assumed. The buckled shape of honeycomb cells is found to be a modified form of a developable surface into which a circular cylinder can deform. This modified shape is a function of the effective glue line width between adjacent honeycomb cells in the honeycomb pad. Details of these derivations are given in the Appendix.

Once analytical expressions for the deflections in the buckled shape are available, an energy method can be used for computing buckling loads.

PROCEDURE

A single honeycomb cell will be considered because it is simpler to study analytically the response of single cells than it is to study clusters of cells. Furthermore, individual cells may be responding differently depending on their physical location in the honeycomb composite. In experimental investigations it is simpler to study the behavior of groups or clusters of cells. The buckled shape of a honeycomb cell resembles the developable polyhedral surface which has slope discontinuities or zero radii of curvature as shown in Fig. 3b. The actual buckled cylinder with a finite thickness has folds which are more rounded. The roundness of the corners at the folds increases as the cylinder thickness increases.

Theoretically, a function with slope discontinuities or infinite curvature can be exactly represented by a Fourier series with an infinite number of terms (constrained only by the Dirichlet conditions).⁶ If this Fourier series is truncated it will represent a surface with a finite curvature at the position of the original slope discontinuities. The curvature at the folds increases with the number of terms retained in the series.

If the exact displacement equations could be represented identically by a Fourier series with an infinite number of terms, there would be zero extensional strain energy but infinite bending moment for elastic bending at the fold edges for the model shown in Fig. 3b. This Fourier series when truncated to a finite number of terms, should provide a good representation of the deflection shape of a buckled finite thickness cylinder. An increasing number of terms would be required as the cylinder wall becomes thinner. This is because the thinner the buckled cylinder, the closer it approaches the developable shape assumed by a buckled infinitely thin circular cylinder. Increasing the number of Fourier series terms used would also decrease the extensional strain energy and increase the bending strain energy. For an infinite number of terms the extensional strain energy vanishes and the bending strain energy approaches infinity.

One way to obtain the buckling load in a static analysis is to set the external work done on the cylinder equal to the total strain energy in the cylinder. This will in general not be the minimum buckling load. To obtain the minimum the number of terms in the Fourier series for the deflections is varied until a sufficient number of buckling loads has been computed to establish the minimum. The buckled shape is determined by the number of terms included in the series.

1. Developable Surface Deflection Shape

Since the buckled shape of a cylinder has symmetry and periodicity in the circumferential coordinate θ and the axial coordinate x , as shown in Fig. 4, only the deflections of one panel are necessary to obtain the coefficients for the Fourier series representation of the displacements when suitable coordinate transformations are made. The derivations of the exact radial and tangential displacement expressions are given in Section 1 of The Appendix. Eqs. (1.11) and (1.12), the expressions for the radial and tangential displacements necessary to transform a circular cylindrical shell into a developable polyhedral surface show that there is a simple relation between the tangential displacement and the first derivative of the radial displacement. This allows the tangential displacement to be expressed approximately in terms of the Fourier series expansion of the radial displacement. Then there is no necessity for determining the Fourier coefficients for the tangential displacement.

The radial displacement functions are expanded in a double Fourier series in θ and x in the following manner. First, the two derived functions of the exact radial displacement w , with limits as a function of x , are represented by a single Fourier series expansion in the circumferential coordinate θ . This Fourier series has coefficients a_j which are a function of x . The formula for the a_j coefficients is determined by integrating the derived exact radial displacements over two regions of θ which have limits that depend on x .

$$W(x, \theta) = \sum_{j=0}^{\infty} a_j(x) \cos jn\theta$$

The deflected shape obtained has slope discontinuities in the axial direction, but with a finite number of terms in this expansion there is no slope discontinuity in the circumferential direction. These $a_j(x)$ Fourier coefficients are themselves now represented by a Fourier series in terms of x , such that

$$a_j(x) = \sum_{i=0}^{\infty} a_{ij} \cos \frac{im\pi x}{L}$$

or

$$W(x, \theta) = \sum_{j=0}^{\infty} \sum_{i=0}^{\infty} a_{ij} \cos \frac{im\pi x}{L} \cos jn\theta$$

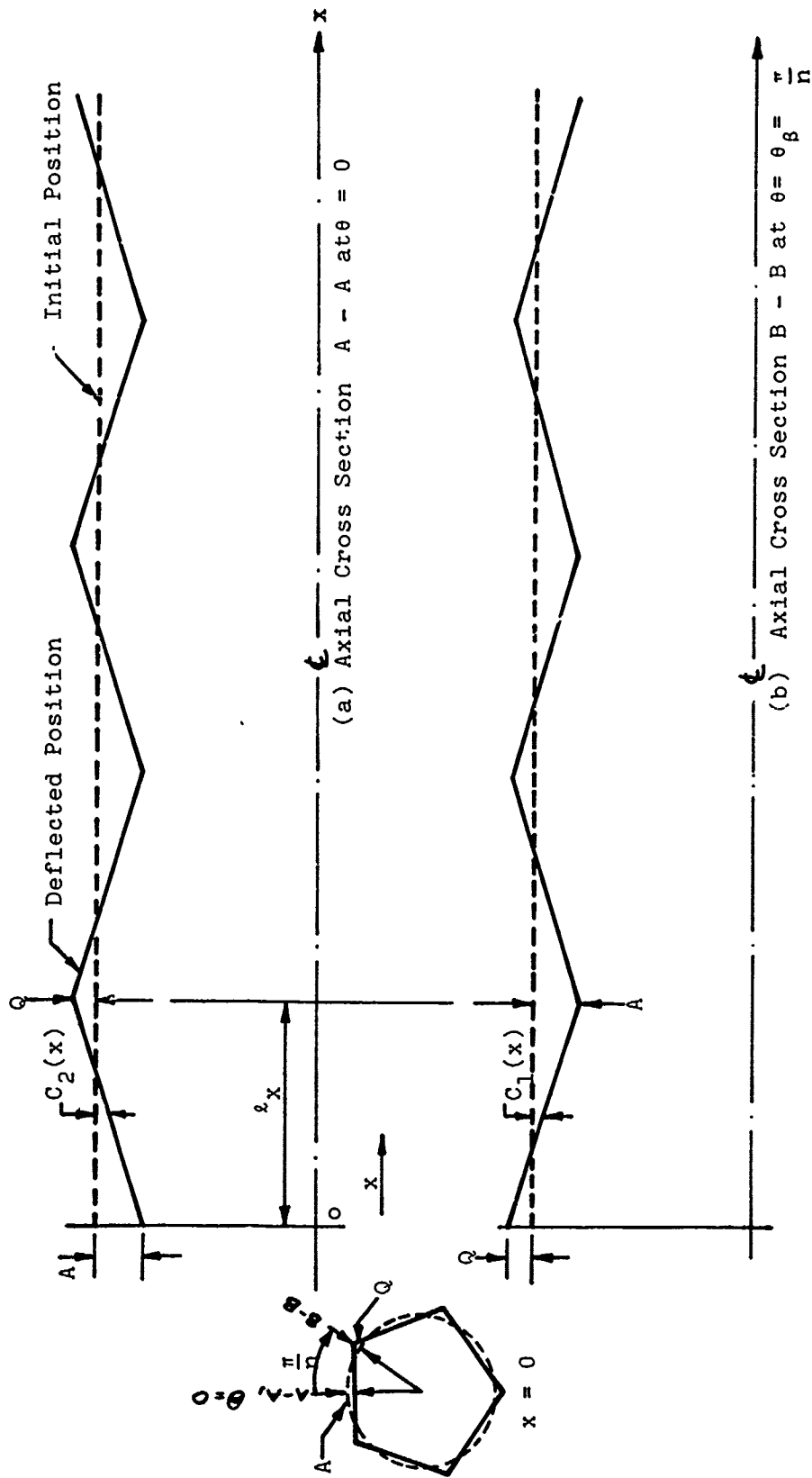


Fig. 4 Axial Cross Sections

The coefficients a_{ij} in this Fourier series are derived as shown in the Appendix. When an infinite number of terms are taken in this Fourier series it yields exact displacement values and slope discontinuities as shown in Fig. 3b. With a finite number of terms in the series there are no slope discontinuities in either the circumferential or axial directions.

A computer program to compute the Fourier coefficients $a_{ij}(x)$ and a_{ij} was written for the CDC 6600 computer. The computer was used to determine the coefficients, plot the surface deformations and compare the Fourier series representation of the radial deflection with the exact values of the radial deflection.

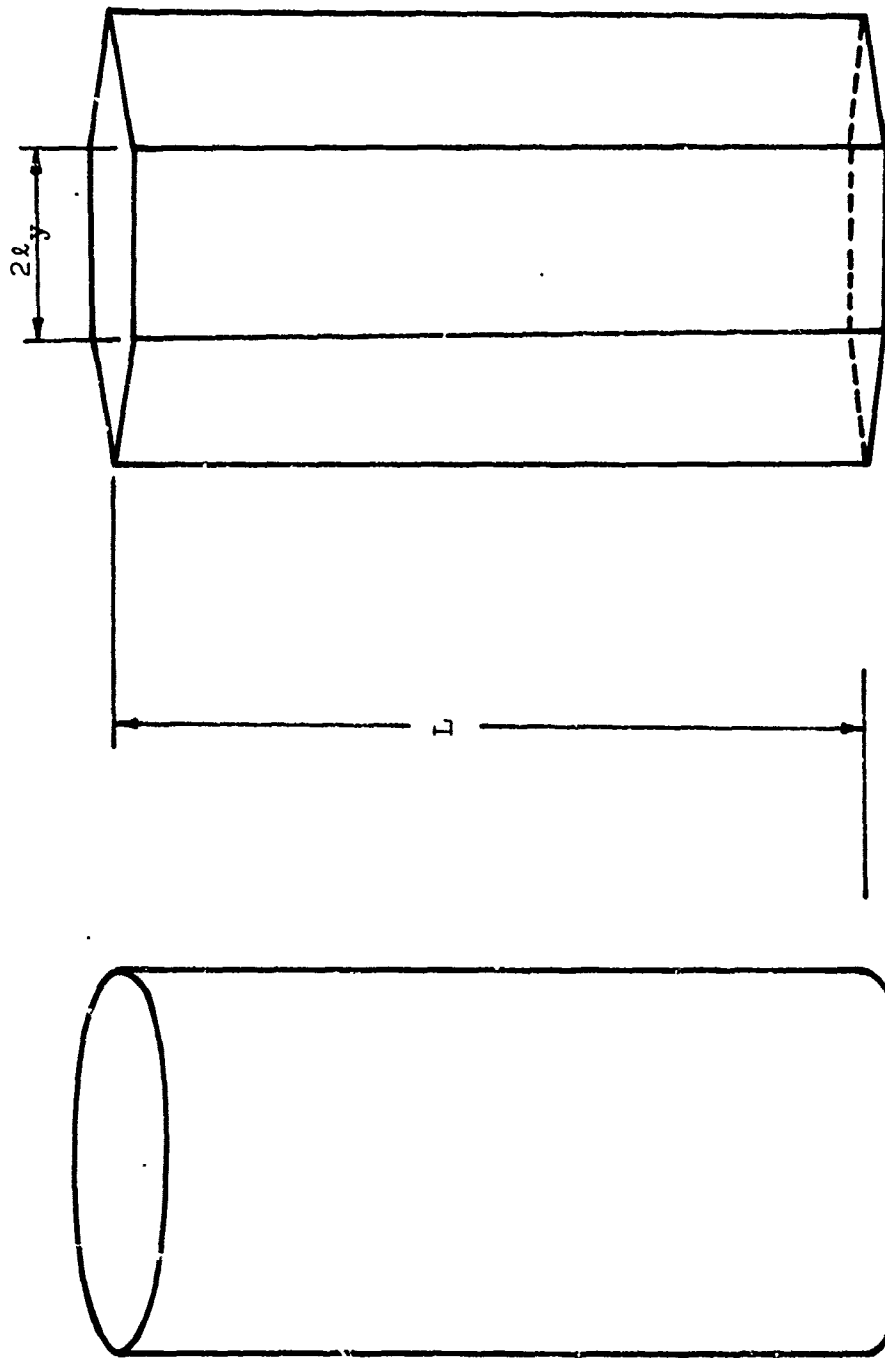
Hoff, Madsen and Mayer⁵ have published formulas for computing approximate values of the Fourier coefficients for large circumferential mode numbers ($n \geq 10$). A computer program was written in order to obtain the values of these approximate coefficients. These approximate coefficients are compared in RESULTS, with the more exact values of a_{ij} referred to above.

2. Honeycomb Deflection Shape

After the coefficients of the Fourier series representation of the radial displacement for the developable shape are obtained, it is possible to determine the radial displacements required to produce the original hexagonal cylindrical shell shape of individual cells of the honeycomb pad. The hexagonal cell is merely the $n=6, m=0$ mode of the circular cylindrical shell as shown in Fig. 5. This shape represents the nearly perfect hexagonal shape of precision made honeycomb. In mass produced manufactured honeycomb, the cell tends toward a rounded hexagonal shape, which can be more closely represented by a smaller number of terms in the Fourier series for the $n=6, m=0$ mode.

During this work, to establish the nature of the buckling pattern in crushed honeycomb, an impact test was performed in which the honeycomb pad was cut into four pieces prior to testing. The cuts were made along the cell edges and then the four cut pieces were butted together for the test. This approach was used to avoid the distortion in the buckle pattern which cutting after testing usually produces. Three of the pieces illustrating the test configuration are shown in Fig. 1. The cell buckle pattern is shown in Fig. 6.

From this photograph it may be observed that the buckling pattern of the cells in the crushed honeycomb is such that the radial displacement from the sides which formed the original hexagonal cross section shape alternates from inward to outward as one progresses around the periphery of the cell wall and the maximum displacements appear to be equal.



Initial Circular Cylinder

$n = 0, m = 0$

Hexagonal Cylinder

$n = 6, m = 0$

Fig. 5 Initial Circular Cylinder and Hexagonal Cylinder

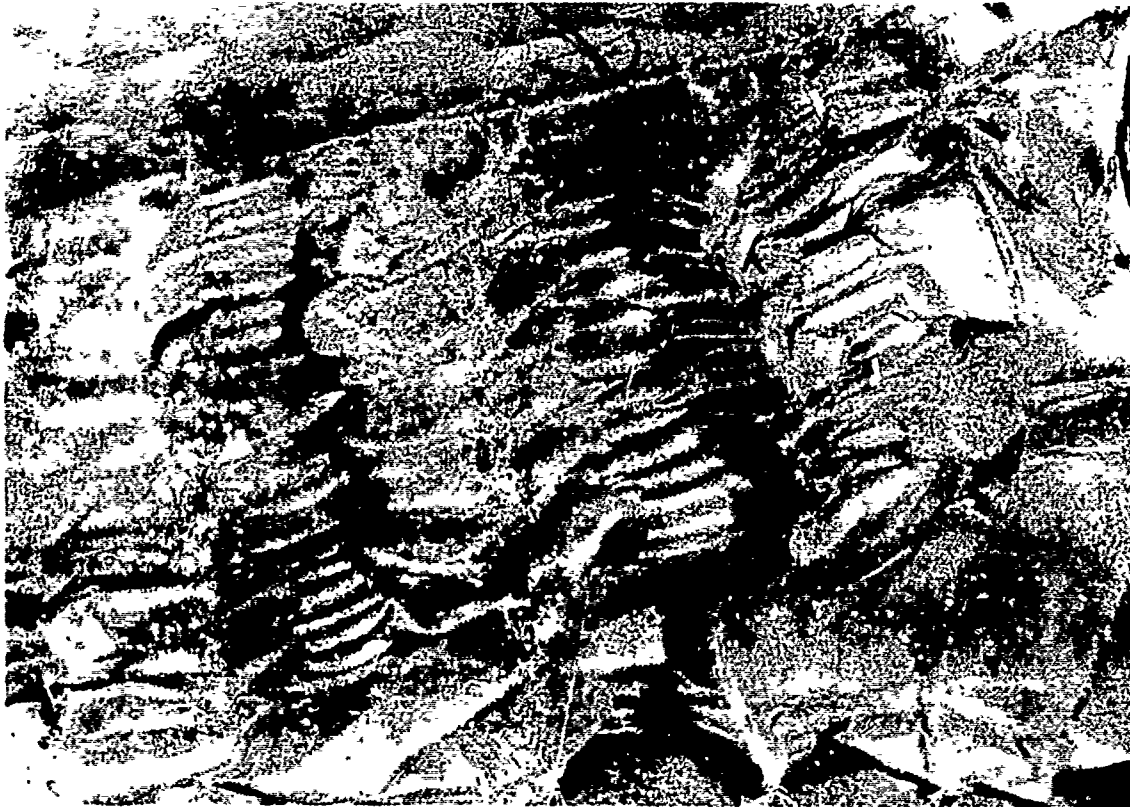


Fig. 6 Honeycomb Cell Displacement
Pattern After Crushing

As mentioned previously, the initial honeycomb hexagonal shape is equivalent to the $n=6, m=0$ mode of a circular cylinder. Cross sections of a buckled cylindrical shell in the $n=3$ mode have three sides which form an equilateral triangle at the axial nodes. However, there are six sides at any cross section between the axial nodes. Maximum displacements occur at the circumferential midpoints of the original sides of the hexagon as shown in Fig. 7. From the exact equations for the radial displacements it is found that the difference between the maximum inward deflection at these points for the $n=3$ mode and the $n=6, m=0$ mode, is equal to the maximum outward deflection. Thus the alternating inward and outward displacements observed in Fig. 6 can be regarded as the displacements of a circular cylindrical surface in a modified $n=3$ buckling mode minus the $n=6, m=0$ mode which represents the original hexagonal cylindrical shape of the cell shown in Fig. 5.

The shape of the modified $n=3$ buckling mode of the honeycomb cells is found to be a function of the width of the glue line bonding adjacent cell walls which remains intact during buckling, that is, the "effective glue line width." The cross section of a buckled circular cylindrical shell at the midpoint ($l_x/2$ in Fig. 7) between the axial nodes of the $n=3$ buckling mode is a regular hexagon. If there is no extension of surfaces this section for the $n=3$ mode must be the same as the cross section for the $n=6, m=0$ mode. Thus there is no change from the original hexagonal shape. The axial location of this section corresponds to the axial nodes of a buckled honeycomb pad cell. The ends of the honeycomb cells where displacements are constrained to the hexagonal cross section shape by the facing paper will always be axial nodes.

It is very difficult to tell by examination of buckled honeycomb exactly what the geometry of the buckled cell is. Clearly there are alternating inward and outward radial deflections. However, the hexagonal cells are restrained at 4 points, i.e., there are 4 glue lines, not three as shown in Fig. 8. Two of the four glue lines act as point restraints rather than lines. Thus it seems very certain that the buckling pattern cannot be identical to the one for the $n=3$, or the modified $n=3$ modes. Nevertheless, these shapes which can be represented in a reasonably convenient mathematical form can be used to approximate the buckling behavior of honeycomb cells in a pad, and to obtain an indication of the effects of the restraint offered by the glue lines.

To continue the analysis of the glue line effects it is necessary now to express the radial deflections for the modified $n=3$ mode in an analytical form that can later be used in strain energy calculations. The necessary equation can be obtained by taking the equation given previously for

$w(x, \theta)$, i.e.,

$$w(x, \theta) = \sum_{i=0}^{\infty} \sum_{j=0}^{\infty} a_{ij} \cos \frac{i\pi x}{L} \cos j\theta$$

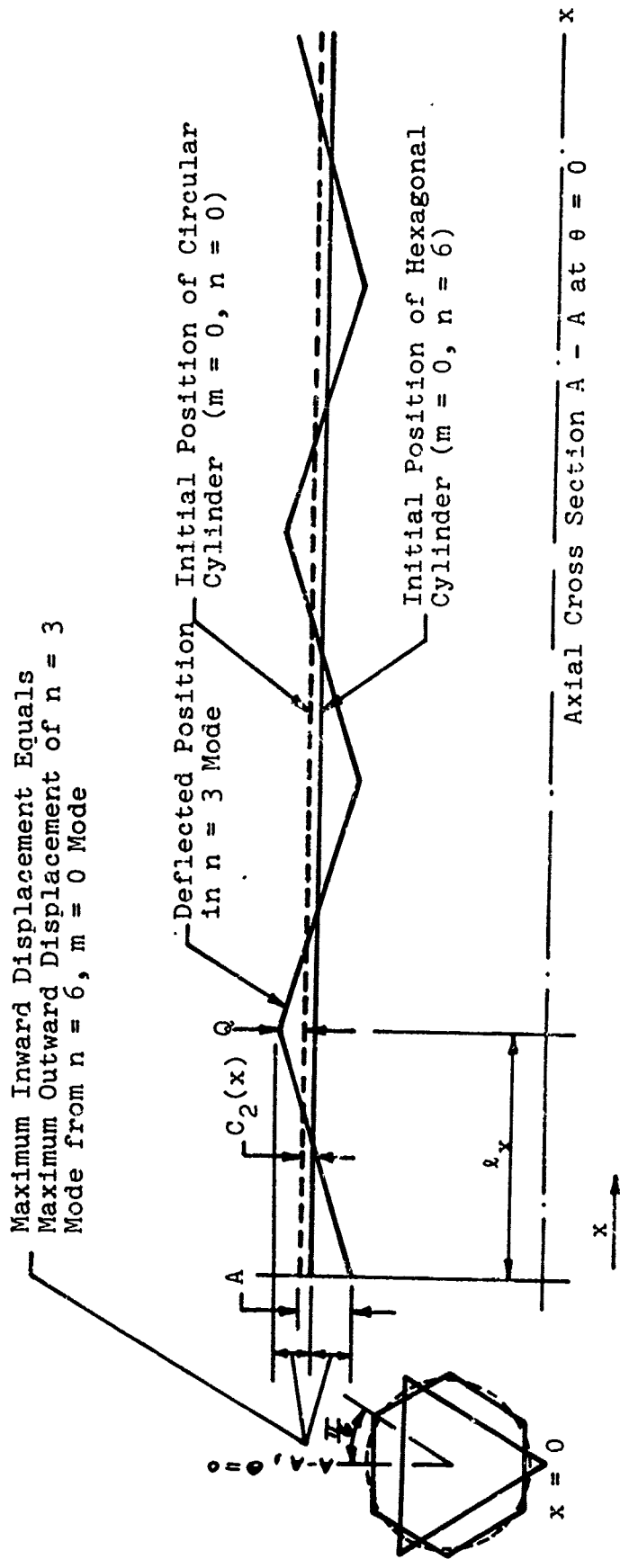


Fig. 7 Profile of Circular Cylinder Buckling in $n = 6, m = 0$, and $n = 3$ Modes

and computing the coefficients a_{ij} for the deflections shown in Fig. 8c for the modified $n=3$ mode. These deflections are obtained by applying purely geometrical considerations and the requirement of no extensions in a developable surface.

When n is specified, the number of folds in the circumferential directions is specified. This does not mean that the paper honeycomb will necessarily buckle in this pattern. Consequently if n is specified all conclusions regarding buckling loads must be predicated on the assumption that the actual buckling pattern will agree with the assumed pattern. The number of longitudinal folds (buckles) is not specified. The more folds or buckles there are the higher the buckling load is likely to be.

It will now be shown that if a cell buckles into the modified $n=3$ mode the effect of the glue line will be to decrease the buckle length, and increase the number of longitudinal folds, and hence the buckling load.

Consider Fig. 8a. This is one of the polyhedral panels of the buckled cell surface viewed normal to the surface. The solid lines indicate a panel for modified $n=3$ buckling, and the dotted lines indicate the shape for the plain $n=3$ mode. For this mode the panel is an equilateral triangle with sides $2\pi a/3$. (The inextensibility conditions requires the total length of three sides to be the same as the circumference of the cylinder, diameter $2a$, from which the developable polyhedral surface is formed.) For the modified $n=3$ mode the triangular panels are changed to trapezoids. If the glue line width is $2b$, as seen in Fig. 8b, the sides of the trapezoid have a length

$$\frac{2\pi a}{3} - 4b$$

as shown in Fig. 8a. The line AB in Fig. 8c is the line AB shown in Fig. 8a. The projection of AB on the horizontal in Fig. 8c is l_x and $l_x = \frac{L}{m}$ where L is the initial length of the cylinder. The horizontal projections of AB and A'B' in Fig. 8c are in the same proportion as the sides of the triangle and the trapezoid in Fig. 8a. Hence

$$\frac{(\frac{2\pi a}{3} - 4b) / \frac{2\pi a}{3}}{1} = \frac{l_x'}{l_x}$$

or $l_x' = (1 - \frac{6b}{\pi a}) l_x$ = the buckle length of the modified $n=3$ mode. The projection of AA' on the horizontal is

the same fractional part of l_x as $2b$ is of $\frac{2\pi a}{3}$, that is, $\frac{3b}{\pi a} l_x$ as shown in Fig. 8c.

To represent the modified $n=3$ mode the double Fourier series for the radial deflection can be obtained from the equation for the $n=3$ mode by simply modifying the argument of the $\cos \frac{i\pi x}{a}$ term to take into account the change in the periodic interval which the glue line causes. Thus for the modified $n=3$ mode

$$W_3(x, \theta) = \sum_{i=1}^{\infty} \sum_{j=1}^{\infty} a_{ij} \cos \frac{i\pi x_1}{(1 - \frac{6b}{\pi a}) l_x} \cos 3j\theta$$

where $x_1 = x - \frac{3b}{\pi a} l_x$

The coordinate transformation is introduced to put the origin of the coordinate system at point A', the fold in the buckling pattern.

The complete derivation of the expressions for the a_{ij} coefficients is given in section 4 of the Appendix.

3. Buckling Stress

The Fourier series expansion for the net deflection of the buckled honeycomb cell is inserted in the bending and stretching strain energy equations as shown in Section 5 of the Appendix. To obtain a buckling stress the sum of the bending and stretching strain energies is equated to the work done by the applied axial force up to the time the buckling pattern is formed. These quantities are each functions of the deflection shape. The deflection shape is also a function of the indices i and j in the double Fourier series. The higher the values of i and j the closer the developable shape is approached. The indices are increased until a minimum buckling stress is obtained. This value represents the stress required to buckle the shell into a particular mode. (In this case the modified $n=3$ mode.)

The non-dimensional buckling stress, σ/E is shown as a function of geometrical parameters t/c , l/c , the glue line width, $2b$, and Poisson's ratio in the RESULTS.

RESULTS

1. Developable Polyhedral Surface Equations--Exact Displacements

The shape of a circular cylinder which has buckled into a polyhedral developable surface is symmetric and periodic in the circumferential coordinate and the axial coordinate x . Thus only the equations of the deflections of a single panel of the buckled surface are initially required to obtain the Fourier series expansion of the displacement of the entire buckled surface when suitable coordinate transformations are made.

The radial and circumferential displacements, w and v respectively, of a single panel have each been determined by purely geometrical analysis as two separate functions of the circumferential coordinate θ and axial coordinate x . Each function is valid in a region whose circumferential coordinate limits are a function of the axial coordinate x . These functions derived in Section 1 of the Appendix are:

$$W(x, \theta) = [a + c_2(x)] \cos \theta + a \theta \sin \theta - a$$

$$0 \leq \theta \leq \left[1 - \frac{x}{l_x}\right] \frac{\pi}{n}$$

$$V(x, \theta) = [a + c_2(x)] \sin \theta - a \theta \cos \theta$$

$$W(x, \theta) = [a + c_1(x)] \cos\left(\frac{\pi}{n} - \theta\right) + \left(\frac{\pi}{n} - \theta\right) a \sin\left(\frac{\pi}{n} - \theta\right) - a$$

$$\frac{\pi}{n} \left[1 - \frac{x}{l_x}\right] \leq \theta \leq \frac{\pi}{n}$$

$$V(x, \theta) = [a + c_1(x)] \sin\left(\frac{\pi}{n} - \theta\right) + \left(\frac{\pi}{n} - \theta\right) a \cos\left(\frac{\pi}{n} - \theta\right)$$

where

$$l_x = \frac{L}{m}$$

$$c_2(x) = \left(\frac{A+Q}{l_x}\right)x - A = \text{Radial Displacement amplitude at } x, \theta = 0$$

$$c_1(x) = Q - A - c_2(x) = \text{Radial Displacement amplitude at } x, \theta = \frac{\pi}{n}$$

and Q and A are the amplitudes of the maximum radial displacement at the longitudinal nodes in the outward and inward directions respectively. The values of the amplitudes given by Coppa² are:

$$\begin{aligned} Q &= \frac{a}{\sin \frac{\pi}{n}} \left[\frac{\pi}{n} - \sin \frac{\pi}{n} \right] \\ A &= \frac{a}{\sin \frac{\pi}{n}} \left[\sin \frac{\pi}{n} - \frac{\pi}{n} \cos \frac{\pi}{n} \right] \end{aligned} \quad (1)$$

From Eqs. (1) and (2) it may be seen that there is a simple relationship between the tangential and radial displacements. The tangential displacements can be expressed in the following manner:

$$v(x, \theta) \begin{cases} = -\frac{dw}{d\theta} + a \sin \theta & 0 \leq \theta \leq \frac{\pi}{n} \left[1 - \frac{x}{L_x} \right] \\ = -\frac{dw}{d\theta} + a \sin \left(\frac{\pi}{n} - \theta \right) & \frac{\pi}{n} \left[1 - \frac{x}{L_x} \right] \leq \theta \leq \frac{\pi}{n} \end{cases}$$

a. Fourier Coefficients of Double Fourier Series

The derived radial displacement functions w given in Eq. (1) are expanded into a double Fourier series in θ and x as follows. Complete details of the expansion are given in section 2 and 3 of the Appendix.

First the two functions of radial displacement w given in Eq. (1) are represented by a single Fourier series expanded in θ . The Fourier coefficients a_j are a function of x.

$$w(x, \theta) = \sum_{j=0}^{\infty} a_j(x) \cos jn\theta$$

The deflected shape obtained has slope discontinuities in the axial direction, but with a finite number of terms in this expansion there is no slope discontinuity in the circumferential direction.

The $a_j(x)$ coefficients are determined by integrating the two functions of w from Eqs. (1) and (2) over the two applicable regions of $\theta(x)$ as presented in Section 2 of the Appendix. The equation derived is:

$$a_j(x) = \left(1 - \frac{1}{2} \delta_j^0 \right) (-1)^j \frac{2n}{\pi} \left[\begin{aligned} & \left(1 - \cos \frac{\pi}{n} \right) \left(\frac{\sin E\theta_{\theta 1}}{E^2} + \frac{\sin F\theta_{\theta 1}}{F^2} \right) \\ & + \sin \frac{\pi}{n} \left(\frac{\cos E\theta_{\theta 1}}{E^2} + \frac{\cos F\theta_{\theta 1}}{F^2} \right) \end{aligned} \right] a \delta_j^0 \quad (2)$$

where

$$E = 1 + jn$$

$$F = 1 - jn$$

$$\theta_{m1} = \frac{m\pi x}{nL}$$

These $a_j(x)$ Fourier coefficients are expanded in a Fourier series in terms of x in Section 3 of the Appendix such that

$$a_j(x) = \sum_{i=0}^{\infty} a_{ij} \cos \frac{im\pi x}{L}$$

or

$$w(x, \theta) = \sum_{j=0}^{\infty} \sum_{i=0}^{\infty} a_{ij} \cos \frac{im\pi x}{L} \cos jn\theta \quad (8)$$

An infinite number of terms in this series gives the deflection of a developable surface with slope discontinuities at the surface folds. However a finite number of terms represents folds with finite radii of curvature.

The formula for the Fourier coefficient a_{ij} is obtained by integrating the Fourier coefficient $a_j(x)$ in the region of one axial half wave length by taking into consideration the symmetry of the deflections in the axial direction. This derivation is given in detail in Section 3 of the Appendix. The equation is

$$a_{ij} = \frac{\left[\frac{[1 + (-1)^{i+j}] (-1)^i \left[1 - \frac{\delta_j^0}{2}\right] 8a \left\{ \frac{n \sin \frac{\pi}{2n} \right\}^2}{\pi} \right]}{\left[\frac{[1 + 3(jn)^2 - (in)^2]}{[1 - (jn)^2] \{ [1 - (in)^2 + (jn)^2]^2 - 4(jn)^2 \}} \right]} \quad \left(1 - \frac{\delta_i^0}{2}\right) - 2a \delta_j^0 \delta_i^0 \quad (9)$$

2. Computer Check

Numerical values of a_{ij} have been computed and used to plot the profile of the deflections of a circular cylinder buckled in the $n=3$ mode as shown in Fig. 9. Three curves are shown. The labels $I=1,6,19$ indicate the number of i terms in the expansion. Normalized a_{ij} values determined from the derived exact formula can be compared in Table 1 with the values of a_{ij} determined by using the Hoff, et al⁷ approximate formula¹ ($n=10$). For large values of the circumferential mode number n these normalized values are nearly constant for all values of n , and thus essentially independent of n . It can be seen that the values obtained from the approximate formula are very good approximations to the exact values for n greater than 7 or 8. At the lower values of n , there is an appreciable difference.

3. Honeycomb Cell Shape Equations

As indicated previously the buckle shape of crushed honeycomb cells is to be approximated by the modified $n=3$ radial deflection shape. A Fourier series which will represent the shape is

$$w_{n=3 \text{ mod}}(x, \theta) = \sum_{i=0}^{\infty} \sum_{j=0}^{\infty} a_{ij3} \cos 3j\theta \cos \frac{im\pi x}{L(1-\frac{6b}{\pi a})}$$

where b is half the effective glue line width. The expression for the coefficient a_{ij3} is

$$a_{ij3} = \frac{2a(-1)^{i+j} (1-\frac{6b}{\pi a})^0}{[1-\frac{6b}{\pi a}]^2 \pi^2 E \left[\frac{E^2}{9} - \frac{i^2}{(1-\frac{6b}{\pi a})^2} \right]} \times$$

$$\left[\begin{aligned} & [1 - \cos \frac{\pi}{3}] [-(-1)^j \cos(\frac{Eb}{a} - \frac{\pi}{3}) + (-1)^i \cos \frac{Eb}{a}] \\ & + \sin \frac{\pi}{3} [-(-1)^j \sin(\frac{Eb}{a} - \frac{\pi}{3}) - (-1)^i \sin \frac{Eb}{a}] \\ & + \text{same thing with } F \text{ for } E \end{aligned} \right] - a \delta_j^0 \delta_i^0$$

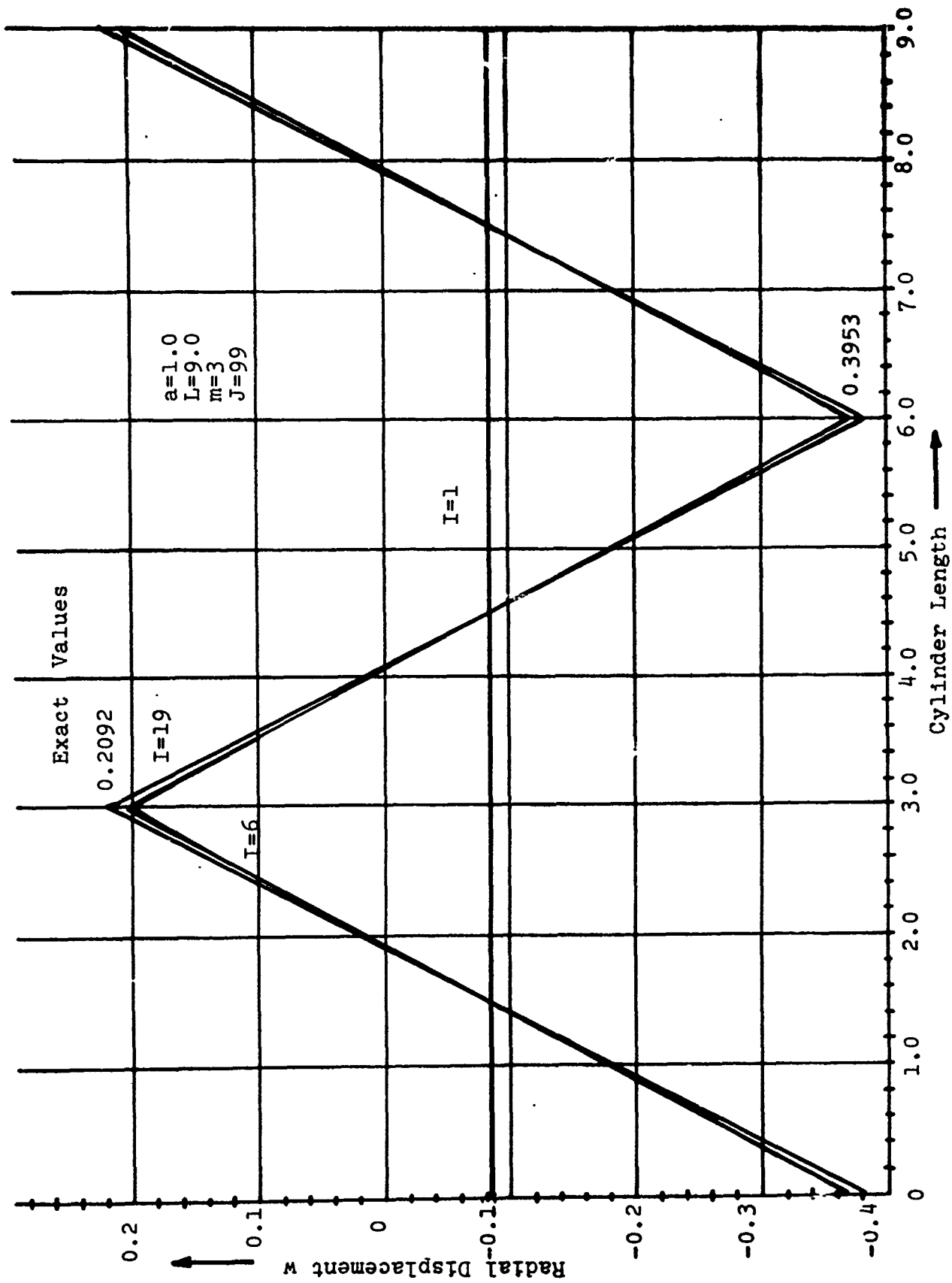


Fig. 9 Radial Displacement at $\theta=0$ for Different Values of I

$$A_{ij} = \frac{n^2}{a} a_{ij}$$

n	A ₀₀	A ₁₁	A ₁₃	A ₃₁	A ₀₂	A ₂₀	A ₂₂	A ₃₃
2	0.7577	2.5938	-0.0412	0.1052	0.0942	0.4323	-0.4529	0.1892
3	0.7930	2.2276	-0.0193	0.0435	0.0417	0.4690	-0.4788	0.2071
4	0.8057	2.1224	-0.0110	0.0240	0.0235	0.4824	-0.4880	0.2136
5	0.8117	2.0768	-0.0072	0.0152	0.0150	0.4887	-0.4923	0.2167
6	0.8150	2.0528	-0.0050	0.0105	0.0208	0.4921	-0.4947	0.2184
7	0.8170	2.0385	-0.0037	0.0077	0.0153	0.4942	-0.4961	0.2194
8	0.8183	2.0294	-0.0028	0.0059	0.0117	0.4955	-0.4970	0.2200
9	0.8191	2.0231	-0.0022	0.0046	0.0093	0.4965	-0.4976	0.2205
10	0.8198	2.0187	-0.0018	0.0038	0.0038	0.4971	-0.4981	0.2208
20	0.8218	2.0046	-0.0005	0.0009	0.0009	0.4993	-0.4995	0.2219
100	0.8224	2.0002	-0.0000	0.0000	0.0000	0.5000	-0.5000	0.2222
From Ref.5 all n>10	0.823	2.000	-0.0000	0.0000	0.0000	0.5000	-0.5000	0.2222

n	A ₄₀	A ₄₄	A ₅₅	A ₆₀	A ₆₆	A ₈₀	A ₁₀₀	A ₁₂₀
2	0.1029	-0.1041	0.0663	0.0454	-0.0456	0.0254	0.0163	0.0113
3	0.1148	-0.1154	0.0735	0.0508	-0.0509	0.0286	0.0183	0.0127
4	0.1192	-0.1195	0.0763	0.0529	-0.0529	0.0297	0.0190	0.0132
5	0.1212	-0.1215	0.0776	0.0538	-0.0539	0.0303	0.0194	0.0134
6	0.1224	-0.1225	0.0783	0.0543	-0.0544	0.0306	0.0196	0.0136
7	0.1231	-0.1232	0.0788	0.0547	-0.0547	0.0307	0.0197	0.0137
8	0.1235	-0.1236	0.0791	0.0549	-0.0549	0.0309	0.0198	0.0137
9	0.1238	-0.1239	0.0793	0.0550	-0.0550	0.0309	0.0198	0.0137
10	0.1241	-0.1241	0.0794	0.0551	-0.0551	0.0310	0.0198	0.0138
20	0.1248	-0.1248	0.0799	0.0555	-0.0555	0.0312	0.0200	0.0139
100	0.1250	-0.1250	0.0800	0.0555	-0.0555	0.0313	0.0200	0.0139
From Ref.5 all n>10	0.1250	-0.1250	0.0800	0.0556	-0.0556	0.0313	0.0200	0.0139

Table 1 Comparison of Fourier Coefficients

The values of a_{ij} coefficients have been computed. To test their validity the deflection shape produced by using the a_{ij} coefficients for the degenerate case of zero width glue line has been compared to the displacement shape produced by the a_{ij} coefficients in the $n=3$ mode. The two displacements agree.

The net displacement of a buckled honeycomb cell is equal to the Fourier series expression for the displacements for the modified $n=3$ buckling shape minus the original hexagonal cross sectional shape which is the $n=6, m=0$ mode. Since the original hexagonal shape is in the $m=0$ mode, the displacement shape is not a function of x .

The original hexagonal cross sectional shape cylinder has non zero i and j terms when expanded in $6j\theta$, but when the hexagonal shape is expanded in $3j\theta$ the odd j terms equal zero, as shown in Section 4 of the Appendix. The net deflection is expressed in the form

$$w_{net} = \sum_{j=0}^{\infty} \sum_{i=0}^{\infty} \left[a_{ij} \cos \frac{im\pi x}{L(1-\frac{6b}{\pi a})} - \frac{[1+(-1)^j]}{2} a_{ij} \right] \cos 3j\theta$$

4. Buckling Stress

As indicated in the previous section the buckling stress is determined by using the expression for the net deflection to compute bending and stretching strain energy. A computer program was written to determine the strain energies and the external work done by the applied load. These values were then used to compute the minimum buckling stress, as shown in Section 5 of the Appendix. Buckling stress increases with cell wall thickness and increased effective glue line width as shown in Fig. 10. In this figure the buckling stress is shown in non-dimensional form by dividing by Young's modulus E . Cell wall thickness t is non-dimensionalized by dividing by the cell wall width c . Note that the buckling stress increases very rapidly with thickness for thin cell walls (assume c is constant) at small values of t/c , and much less rapidly after t/c exceeds 0.02. The analysis which has been provided is most applicable for thin wall cells and becomes less accurate as the wall thickness increases. This is because the cells will tend to buckle in modes which do not represent developable surfaces as the wall thickness increases. The difference in the buckling patterns is readily observed by loading cylindrical shells of different wall thicknesses until they buckle.

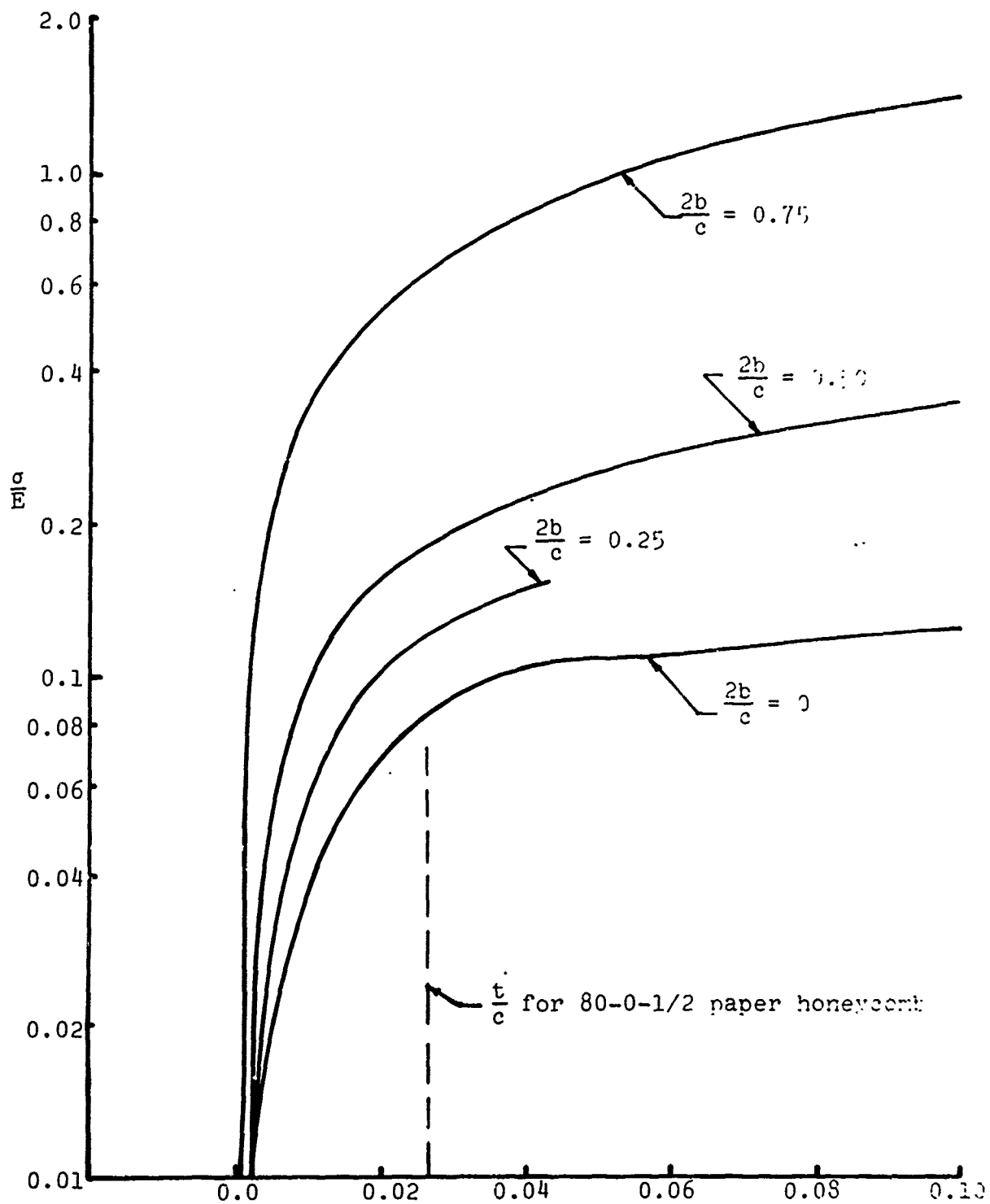


Fig. 10 Buckling Stress Variation with Cell Thickness

Note also, in Fig. 10, the significant increase in buckling stress as the glue line width is increased. The same effect is produced by decreasing the cell size. The results in Fig. 10 are for one axial buckle length ($\lambda/c = 1.0$). However, increasing the glue line width increases the buckling stress significantly at other values of the buckle length (λ/c). This is shown in Fig. 11. The upper group of curves in Fig. 11 indicate that for a constant effective glue line width, the buckling stress increases as the value of λ/c decreases, or as the buckle length becomes shorter and shorter. However, the lower group of curves ($\lambda/c = 4.0$ and $\lambda/c = 10$) show a reversal of this trend. Although this behavior seems at first glance contradictory it is in fact what one might expect. There is a buckle length at which the buckling stress will have a minimum value and this is the buckle length which will be observed no matter what the cell length is. If this were not the case the buckle length for minimum buckling stress would always be determined by the overall length of the cell. It has often been observed that if the loading of a cell is stopped soon enough a number of folds (with a short buckle length) will be formed somewhere along the cell, usually near one end or the other, and the rest of the cell will be unbuckled. This phenomenon has been observed for both static and dynamic loading. The results in Fig. 11 were computed by assuming that the loaded cell would buckle at some arbitrary value of λ/c . Hence these results should not be interpreted to mean that buckling will occur at any of these values of λ/c shown. It can be said, however, that for $t/c = 0.001$ if an axial load is applied and slowly increased until buckling occurs the buckling length will be bounded by the inequality $1 < \lambda/c < 10$. It should be noted that for 80-0 - 1/2 honeycomb the value of c is approximately 0.25in, and t is approximately 0.007in. Thus $t/c = 0.028$ and for $\lambda/c = 4$, $\lambda = 1.0$ in. This value of λ , the buckle length, is appreciably greater than the values that have been observed. A possible explanation of the discrepancy might be that the preferred buckle length (minimum buckling stress) is sensitive to the value of t/c , and the results would therefore have been considerably different had $t/c = 0.028$ been used in the computations. A more likely explanation is that the discrepancy is simply a result of extrapolating from an idealized situation in which the honeycomb cell is uniform in all respects and is assumed to behave elastically right up to the time of buckling, to the real situation in which the cell is far from uniform in all respects and buckling is more plastic than elastic. The results should be interpreted as simply an indication of how the buckling stress is affected by the various parameters, rather than an indication of the buckling stresses and buckling lengths that might be expected under a given set of circumstances.

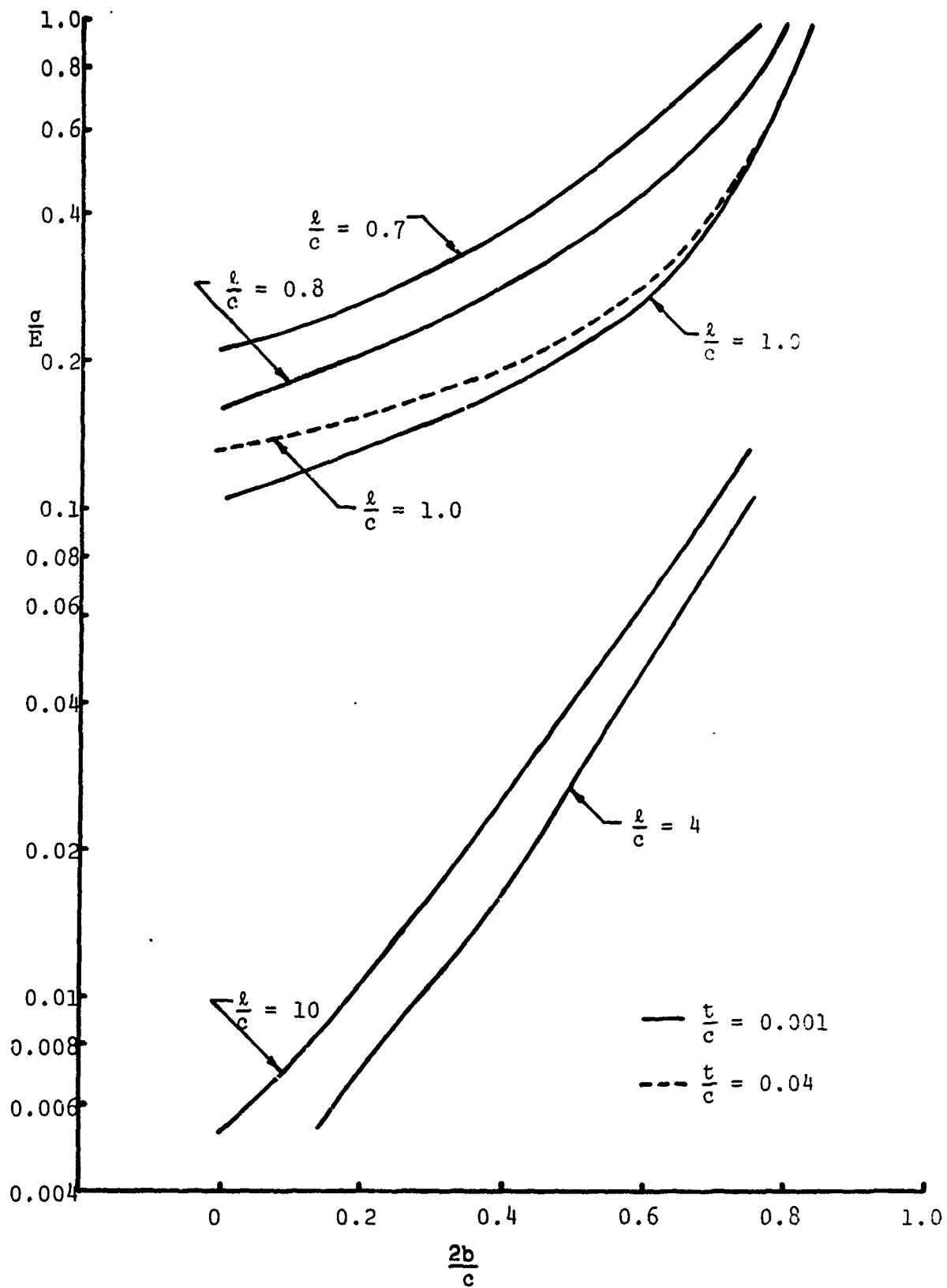


Fig. 11 Buckling Stress Variation with Glue Line Width

As indicated previously a constrained axially loaded hexagonal cell in a honeycomb pad buckles in a modified form of the $n=3$ mode shape. There are six buckles in the circumferential direction. Except at the axial nodes, three of the buckled sides each contain two of the straightened out axial folds produced in the construction of the original hexagonal cell. The maximum number of buckles in the axial direction can be estimated from the L/a ratio using the following expression:

$$\frac{(A+Q)}{\frac{L}{m}} \leq 1$$

$$m \leq \frac{L}{(A+Q)} = \frac{Ln}{2\pi \left(\frac{1}{\sin \frac{\pi}{n}} + \frac{1}{\tan \frac{\pi}{n}} \right)}$$

$$m \leq 1.68 \frac{L}{a}$$

This expression is obtained by considering the limiting value of the sine of the angle formed by the buckled cell wall panel and the original cell wall.

For comparison it may be noted that the crushed honeycomb cell in Fig. 6 has an

$$\frac{L}{a} = 12$$

Hence

$$m \leq 1.68 \frac{L}{a} = 21$$

From the photograph about 19 buckles can be counted along the cell length.

Poisson's ratio for paper is not very well known. To determine its influence on the buckling stress of paper honeycomb the computational results shown in Fig. 12 were obtained. Obviously Poisson's ratio has an insignificant effect on the buckling stress.

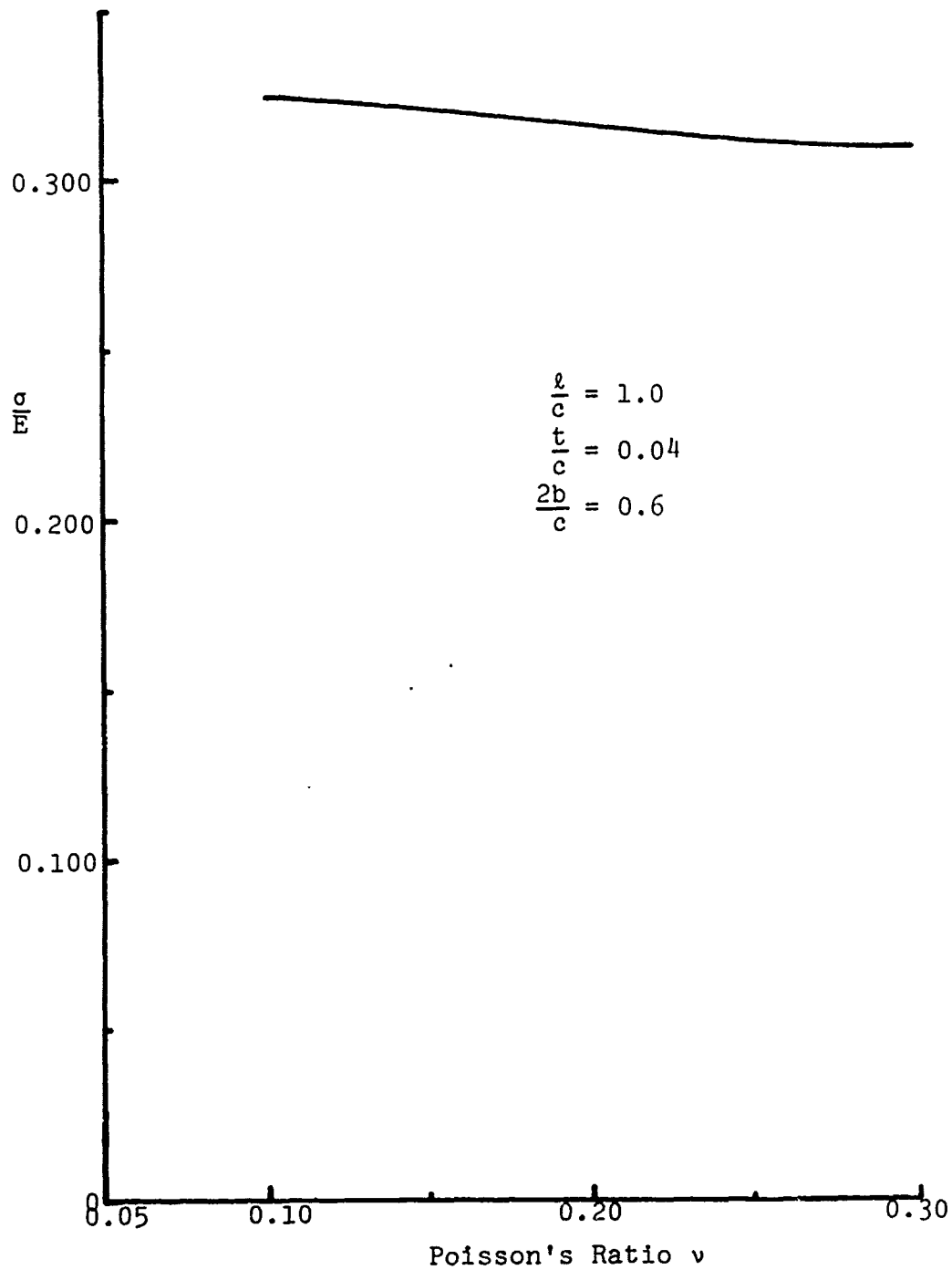


Fig. 12 Buckling Stress Variation with Poisson's Ratio

CONCLUSIONS AND RECOMMENDATIONS

Conclusions

1. Hexagonal paper honeycomb cells buckle under axial loading into a pattern which approaches a developable surface for very thin walls, and departs more and more from that type of surface as the thickness of the cell walls increase.

2. The effective glue line width between adjacent honeycomb cells has a significant effect on the buckling stress of thin wall honeycomb cells.

3. Variations in the effective glue line width have a greater effect on the buckling stress when the effective width is near the maximum value it can have, i.e., the cell wall width.

4. The cell buckling stress increases very rapidly with wall thickness at thicknesses less than $0.02c$ and much less rapidly at greater wall thicknesses.

5. The buckling stress increase with wall thickness becomes more pronounced as the effective glue line width increases.

6. Changes in Poisson's ratio have an insignificant effect on the buckling stress.

7. Honeycomb pads containing hexagonal cells constrained by other hexagonal cells buckle in a modified form of the circumferential mode number $n=3$ of a circular cylindrical shell.

8. The approximate Fourier coefficients in the expressions derived for the radial deflections by Hoff, Madsen and Mayers are quite good for surfaces with a large number of circumferential buckles but rather poor when the number of circumferential buckles is small.

9. A more precise analysis of the buckling of hexagonal cells is not justifiable in view of the great differences between the characteristics of an actual cell and the theoretical cell used in analysis.

Recommendations

To obtain a paper honeycomb which has uniform crushing strength, special attention should be given to quality control of the following parameters:

1. Glue line width
2. Cell wall widths
3. Paper thickness

To provide further authentication for this analysis computations should be made of buckling stresses, for additional values of λ/c and t/c . Further carefully controlled experimentation should be done using paper honeycomb with a wider range of values of c and t .

REFERENCES

1. Coppa, A. P., Buckling of Circular Cylindrical Shells Subject to Axial Impact, NASA TND 1510, 1962.
2. Coppa, A. P., Nash, W. A., Dynamic Buckling of Shell Structures Subject to Longitudinal Impact, Air Force Flight Dynamics Laboratory, FDL-TDR-64-65, December 1964.
3. Coppa, A. P., On the Mechanism of Buckling of a Circular Cylindrical Shell Under Longitudinal Impact, GE R605D494, September 1960.
4. Yoshimura, Y., On the Mechanism of Buckling of a Circular Cylindrical Shell Under Axial Compression, NACA TM 1390, July 1955.
5. Hoff, N. J., Madsen, W. A., Mayers, J., "Post-buckling Equilibrium of Axially Compressed Circular Cylindrical Shells," AIAA Journal V4#1, January 1966, pp 126-133.
6. Wylie, C. R., Advanced Engineering Mathematics, McGraw Hill, 1966, Chapter 6.
7. Karman, T. von and Tsien, H. S., "The Buckling of Cylindrical Shells Under Axial Compression," Journal of Aeronautical Sciences, V8, pp 303-312 (1941).
8. Evensen, D. A., "Some Observations on the Nonlinear Vibration of Thin Cylindrical Shells," AIAA Journal V1 #12, December 1963, pp 2857-2858.
9. Novozhilov, V. V., Foundations of the Nonlinear Theory of Elasticity, Graylock Press, 1953, Chapter 1.
10. Timoshenko, S. P., Gere, J. M., Theory of Elastic Stability, McGraw Hill Book Company, 1961, Chapter 8.

LIST OF SYMBOLS

a	radius.
$a_j = a_j(x)$	Fourier coefficient of Fourier series expansion in θ .
a_{ij}	Fourier coefficient of double Fourier series expansion.
a_{ij3}	Fourier coefficient for $n=3$ mode.
$a_{ij6}, a_{ij\frac{6}{2}}$	Fourier coefficients for $n=6$ mode expanded in $6j\theta$ and $3j\theta$ respectively.
\bar{a}	radius vector.
A	maximum inward radial displacement, also a dummy variable.
A_{ij}	Fourier coefficient normalized with respect to n^2/a .
b	half width of effective glue line.
B	dummy variable.
c	buckled honeycomb cell axial half wave length, also cell wall width.
$c_1(x)$	radial displacement at $\theta = \frac{\pi}{n}$.
$c_2(x)$	radial displacement at $\theta = 0$.
E	variable equal to $1 + jn$, Young's modulus.
F	variable equal to $1 - jn$.
h	thickness.
i	axial mode number.
j	circumferential mode number.
k	variable subscript.
l	length
l_x	buckled panel axial length.
l_y	one half buckled panel circumferential length.
L	cylinder length.
m	axial buckle mode number.
n	circumferential buckle mode number.
P	axial load, dummy variable.
Q	maximum outward radial displacement.
r	radius, radial coordinate.
t	thickness.
T	dummy variable.
u, U	axial displacement, axial displacement vector.

$U_b, U_e,$	
U_{tot}	bending, extensional and total strain energies.
v, \bar{v}	tangential displacement, tangential displacement vector.
w, \bar{w}	radial displacement, displacement vector.
w_{net}	net radial displacement of buckled hexagonal cell.
w_H	radial displacement required to buckle circular cylinder into hexagonal cylinder.
$w_{n=3}$	radial displacement in the $n=3$ mode.
$w_{n=3 \text{ mode}}$	radial displacement of honeycomb cell in modified $n=3$ mode.
x	axial coordinate.
x_k	axial coordinate of a particular cross section.
X	general axial location of axial cross sections.
y	tangential coordinate.
\bar{z}	position vector in final coordinate system.
β	angle locating slope discontinuity in final coordinate system.
γ	circumferential period = $2\pi/n$.
δ	total axial displacement of buckled cylinders.
δ_{m}^n	Kronecker delta.
$\epsilon_x, \epsilon_\theta,$	
$\epsilon_{x\theta}$	axial, tangential and shear strains respectively.
θ	initial position polar coordinate at $x = X$.
θ_1	initial position polar coordinate = $\pi/n - \theta$, at $x = \ell_x - X$.
$\theta_\beta, \theta_{\beta 1}$	angles locating slope discontinuity in initial coordinate system θ and θ_1 , respectively.
ν	Poissons ratio.
ξ	final position coordinate system.
ρ	mass density.
σ	buckling stress of honeycomb cell.
ϕ	angle between axial generator and buckled panel.
$,x$	denotes differentiation with respect to x .

APPENDIX

DERIVATION OF EQUATIONS

The analysis of the buckling of a hexagonal honeycomb cell during axial loading requires five consecutive steps. These are:

1. Determination of the exact displacements which transform a circular cylinder into a polyhedral developable surface.

2. Deriving a formula for the coefficients of a Fourier series for the radial deflection expanded in terms of the circumferential coordinate θ .

3. Derivation of a formula for the coefficients of a double Fourier series for expressing the radial deflection in terms of the circumferential coordinate θ and axial coordinate x .

4. Derivation of a formula for the coefficients of a double Fourier series for including in the radial deflection of buckled honeycomb cells the effect of the effective glue line width.

5. Computation of the strain energy in cells buckled in a specified mode and then using this energy to compute the buckling stress for that mode.

These steps will now be discussed in detail.

1. Exact Displacements

The initial coordinate system of a circular cylinder is shown in Fig. 3. A circular cylindrical surface can buckle into a developable polyhedral surface such as the one shown in Fig. 3 which has a circumferential mode number $n=6$ and longitudinal mode number $m=8$. In this polyhedral developable shape there is no extensional strain at any point in the surface.

In order to determine the exact radial and tangential displacements for a circular cylinder that has buckled into a developable surface it is necessary to determine the radial displacement amplitudes as a function of x .

Fig. 4 shows profile views along the longitudinal axis of a general developable surface at angular coordinate locations $\theta = 0$ and $\theta = \pi/n$. The radial deflection amplitudes as a function of x are determined in the following manner:

Consider the longitudinal cross section shape at $\theta = 0$ shown in Fig. 4a. Coppa, from geometrical considerations and the condition of no extensional strain, has shown that the radial deflection maxima are:

$$Q = \frac{a}{\sin \frac{\pi}{n}} \left\{ \frac{\pi}{n} - \sin \frac{\pi}{n} \right\} \quad (\text{outward deflection})$$

$$A = \frac{a}{\sin \frac{\pi}{n}} \left\{ \sin \frac{\pi}{n} - \frac{\pi}{n} \cos \frac{\pi}{n} \right\} \quad (\text{inward deflection})$$

(1.1)

These expressions apply only if the cross section is an equal sided polygon, which it will be at the cross sections where maximum deflections occur. For intermediate sections let $c_2(x)$ be the radial displacement at $\theta = 0$.

Consider $0 \leq x \leq l_x$.

From Fig. 4a, $c_2(0) = -A$, $c_2(l_x) = Q$.

$$c_2(x) = \left(\frac{A+Q}{l_x} \right) x - A \quad (1.2)$$

From Fig. 4b, $c_1(0) = Q$, $c_1(l_x) = -A$.

$$c_1(x) = -\left(\frac{A+Q}{l_x} \right) x + Q = Q - A - c_2(x) = c_2(l_x - x) \quad (1.3)$$

$$\text{Also } c_2(x) = c_1(l_x - x) \quad (1.4)$$

Furthermore, from Fig. 4 it can be seen that $c_2(x)$ and $c_1(x)$ are periodic in x with a period equal to $2l_x$. Fig. A1 shows some cross sections of the developable surface between the axial nodes. Detailed views of the cross sections are shown in Figs. 2a and 2b. Note that the cross sections have $2n$ variable length sides at any location between the axial nodes for $m = 1, 2, \dots, M$. There are six sides corresponding to the circumferential mode number only at the axial nodes, $x = m l_x$, where six of the sides degenerate to zero length, and the six remaining sides are equal to $2 l_y$ or $2 \frac{a}{n}$, since there is no extension from the original surface. Also note that the sides degenerate to zero length in such a manner that it appears that the cross section at an axial node is the same as an adjacent node cross section, except that the sections are rotated π/n radians with respect to each other.

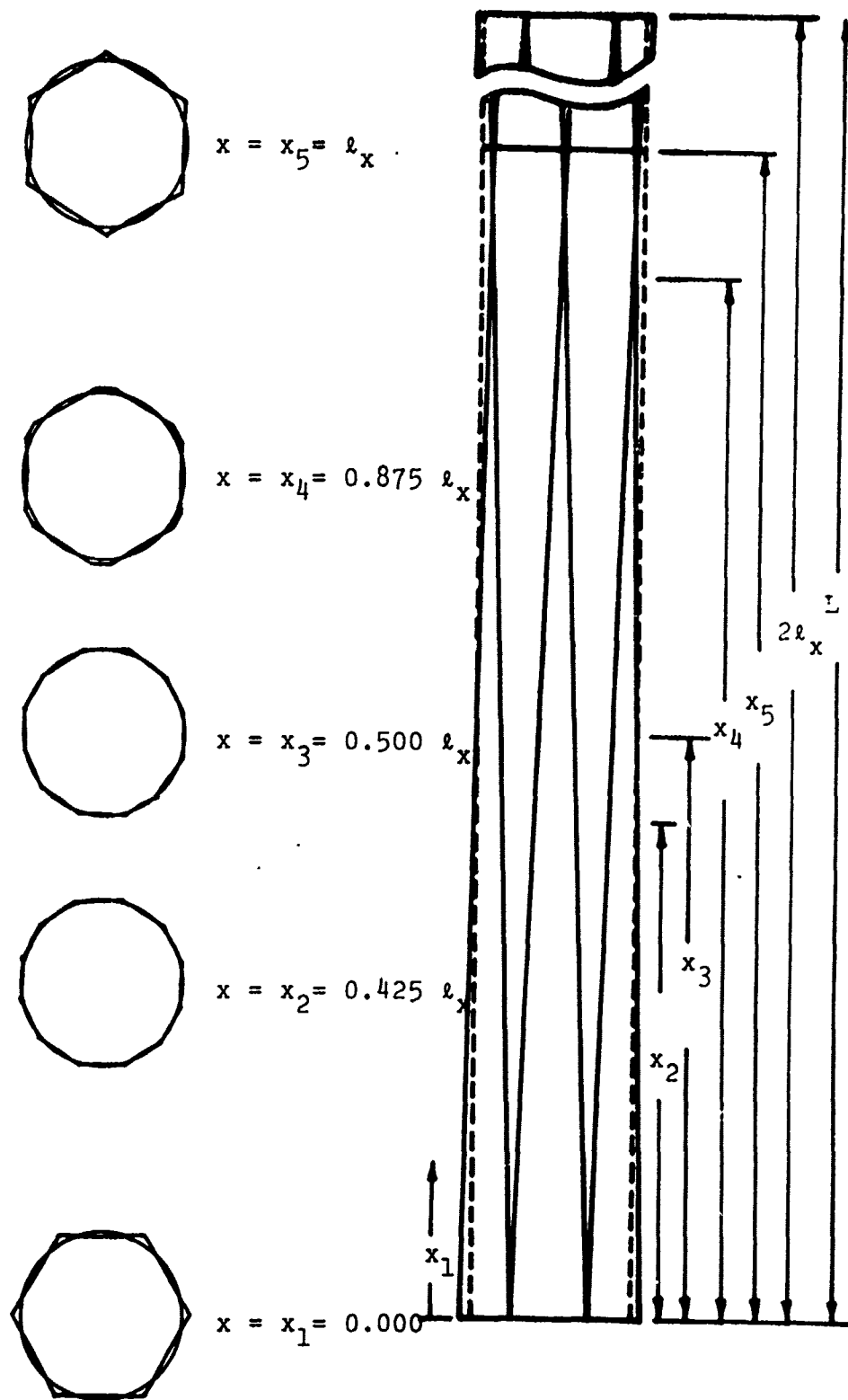
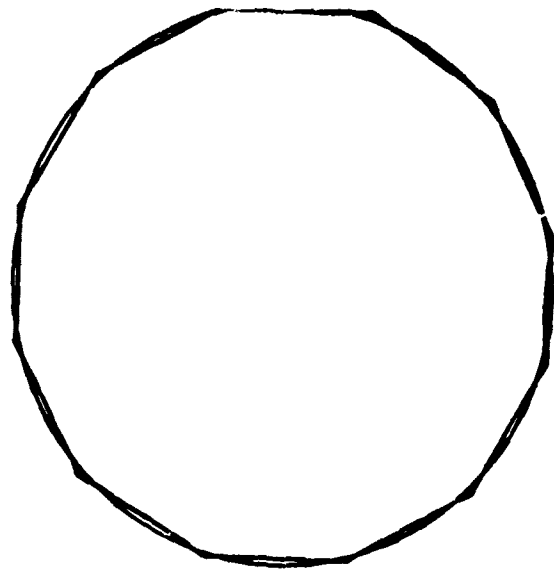
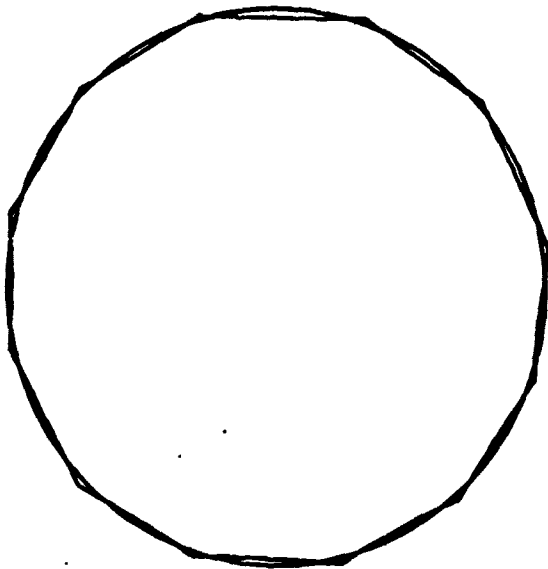


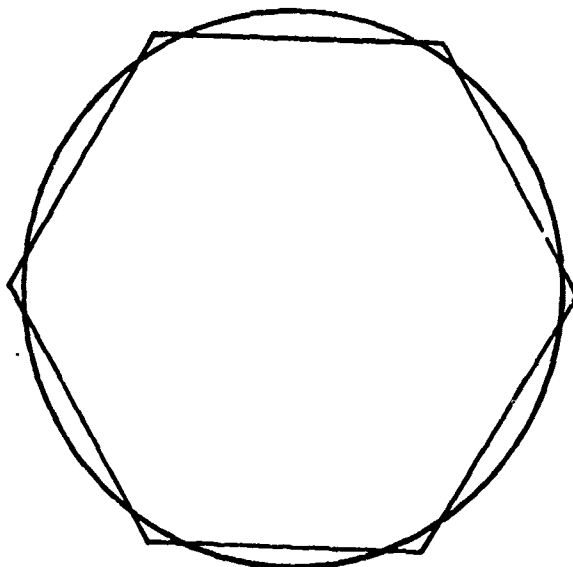
Fig. A1 Cross sections of Deformed Cylinder Between Axial Nodes



$$x = x_3 = 0.500 \ell_x$$

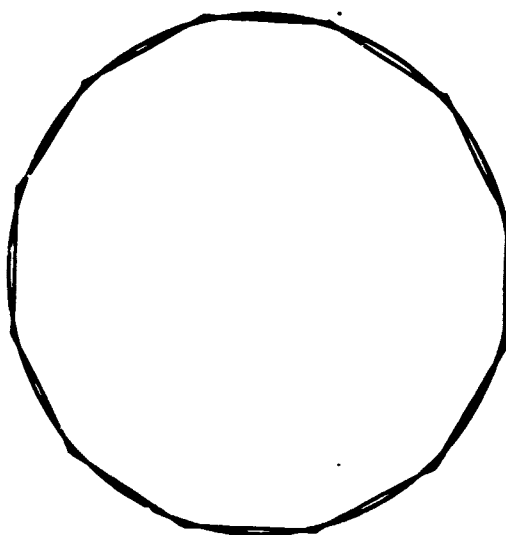


$$x = x_2 = 0.425 \ell_x$$

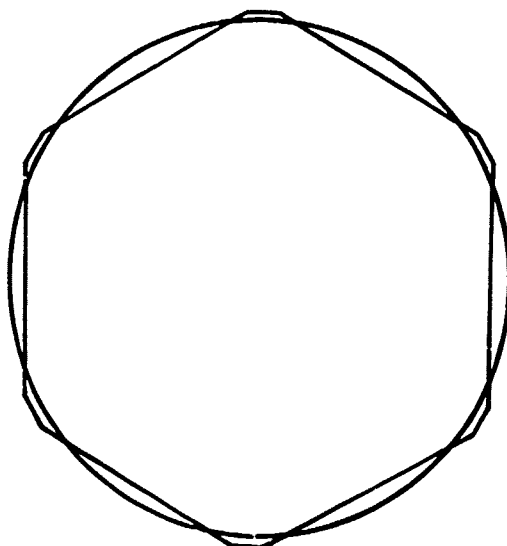


$$x = x_1 = 0.000$$

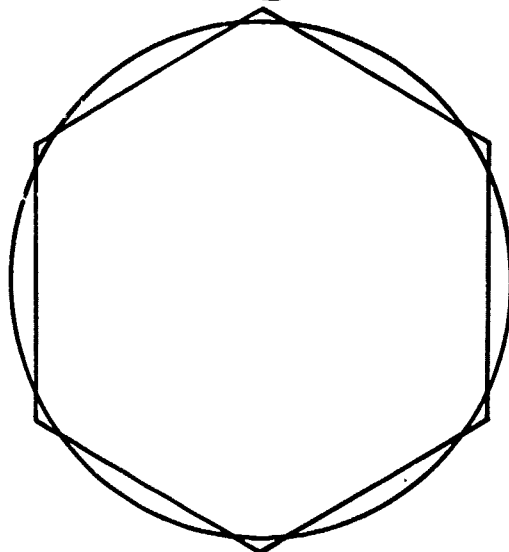
Fig. A2a Detailed Cross Sections of Deformed Cylinder
Between Axial Nodes



$$x = x_3 = 0.500 l_x$$



$$x = x_4 = 0.875 l_x$$



$$x = x_5 = l_x$$

Fig. A2b Detailed Cross Sections of Deformed Cylinder
Between Axial Nodes

Consider now a general cross section of a cylinder buckling in an arbitrary circumferential mode n as shown in Fig. A3. This is an exaggerated view of a portion of a cross section between the axial nodes, such as the cross section shown in the middle of Fig. A2b.

The radial and tangential displacements, w and v , shown change the original cylindrical surface into a polyhedral developable shape. In the initial unbuckled coordinate system θ is the angular coordinate, and ξ is the angular coordinate in the final buckled configuration coordinate system. The angular coordinate locating the limiting edge of one of the sides which is a function of x , is given by the angle $\beta(x)$, measured in the final buckled coordinate system.

Consider first the deflection for $\xi < \beta(x)$ for any general position $x = X$ along the cylinder axis as shown in Fig. A3b.

The initial position point $\theta = \theta_{\beta(x)}$ from which the final position point $\xi = \beta(x)$ is mapped after deflection can be determined as follows:

$$\text{at } \xi = \beta(x),$$

$$\theta = \theta_{\beta}(x)$$

$$\text{and } \tan \xi = \tan \beta$$

For inextensibility

$$\tan \beta = \frac{a \theta_{\beta}}{a + c_2(x)}$$

$$\theta_{\beta} = \frac{[a + c_2(x)] \tan \beta}{a} \quad (1.5)$$

From Fig. A3b

$$\tan \beta = \pm \frac{l_y (1 - \frac{x}{l_x})}{a + c_2(x)} ; \begin{cases} + \text{ for } 0 \leq x \leq l_x; \\ - \text{ for } l_x \leq x \leq 2l_x \end{cases} \quad (1.6)$$

Consider $0 \leq x \leq l_x$

Substituting Eq. (1.6) in Eq. (1.5)

$$\theta_\beta(x) = \frac{[a + c_2(x)]}{a} \frac{l_y (1 - \frac{x}{l_x})}{[a + c_2(x)]} = \frac{l_y (1 - \frac{x}{l_x})}{a}$$

$$\bar{u}(\theta) + \bar{w}(\theta) + \bar{v}(\theta) = \bar{z}(\xi)$$

Consider the deflections for $\xi \leq \beta$, that is, for

$$\theta \leq \theta_\beta = \frac{l_y}{a} \left\{ 1 - \frac{x}{l_x} \right\}$$

$$\begin{aligned} \sum \text{vert projection} &= a \cos \theta + v(\theta) \sin \theta + w(\theta) \cos \theta \\ &= z(\xi) \cos \xi \end{aligned} \quad (1.7)$$

$$\begin{aligned} \sum \text{hor projection} &= a \sin \theta - v(\theta) \cos \theta + w(\theta) \sin \theta \\ &= [a + c_2(x)] \tan \xi \end{aligned} \quad (1.8)$$

Also for inextensibility

$$[a + c_2(x)] \tan \xi = a \theta \quad (1.9)$$

Substituting Eq. (1.9) into Eq. (1.8)

$$a \sin \theta - v(\theta) \cos \theta + w(\theta) \sin \theta = a \theta \quad (1.10)$$

Multiplying Eq. (1.7) by $\cos \theta$ and Eq. (1.10) by $\sin \theta$ and adding yields

$$w(\theta) = [a + c_2(x)] \cos \theta + a \theta \sin \theta - a \quad (1.11)$$

From Eq. (1.10) and (1.11)

$$v(\theta) = [a + c_2(x)] \sin \theta - a \theta \cos \theta \quad (1.12)$$

Note that

$$v(\theta) = -\frac{dw}{d\theta} + a \sin \theta \quad (1.13)$$

Also note

$$w(\theta) = \frac{dv}{d\theta}(\theta) + a \cos \theta - a = \frac{dv}{d\theta} - 2a \sin^2 \frac{\theta}{2} \quad (1.14)$$

Continuity in the circumferential direction at the deformed cylinder ends demands that^{7,8}:

$$\oint \frac{\partial v}{\partial y} dy = \int_0^{2\pi} \frac{\partial v}{\partial \theta} d\theta \equiv 0$$

Eq. 1.12 satisfies this requirement.

The deflections were determined from Fig. A3a in a similar manner for $\beta(x) \leq \xi \leq \frac{Y}{2}$ and were found to be:

$$w(x, \theta) = [a + c_1(x)] \cos\left(\frac{\pi}{n} - \theta\right) + \left(\frac{\pi}{n} - \theta\right) a \sin\left(\frac{\pi}{n} - \theta\right) - a \cos\left(\frac{\pi}{n} - \theta\right)$$

$$\frac{\pi}{n} \left[1 - \frac{x}{l_x}\right] \leq \theta \leq \frac{\pi}{n} \quad (1.15)$$

$$v(x, \theta) = -[a + c_1(x)] \sin\left(\frac{\pi}{n} - \theta\right) + \left(\frac{\pi}{n} - \theta\right) a \cos\left(\frac{\pi}{n} - \theta\right)$$

$$= -\frac{dw}{d\theta} + a \sin\left(\frac{\pi}{n} - \theta\right) \quad (1.16)$$

Eqs. (1.11), (1.12), (1.15), and (1.16) together comprise the exact radial and tangential displacements required for a circular cylindrical surface to form into a developable polyhedral shaped surface. The terminology "exact" is used to distinguish these equations from the series approximation forms which are subsequently used.

The displacement, u , of the developable surface in the axial direction is determined in the following manner. Referring to Fig. A4,

$$u = -x(1 - \cos \phi) = -x(1 - \sqrt{1 - \sin^2 \phi}) \quad (1.18)$$

where

$$\sin \phi = \frac{m}{L} (A + Q)$$

From Eq. (1.1)

$$\sin \phi = \frac{m}{L} \frac{a}{\sin \frac{\pi}{n}} \frac{\pi}{n} [1 - \cos \frac{\pi}{n}]$$

$$\sin \phi = \frac{am\pi}{Ln} \tan \frac{\pi}{2n} \quad (1.19)$$

Inserting Eq. (1.19) in Eq. (1.18) yields

$$u = -x \left[1 - \sqrt{1 - \left(\frac{am\pi}{Ln} \tan \frac{\pi}{2n} \right)^2} \right] \quad (1.20)$$

2. Fourier Series Expansion in θ

The radial deflection given by Eq. (1.11) can be expanded into a Fourier Series in terms of θ in the following manner. Since the radial deflection is periodic in θ with period $2\pi/n$ only the radial deflection between the circumferential nodes is required for the Fourier Series expansion. The radial deflection at any axial location X can be expressed as:

$$w(X, \theta) = \sum_{j=1}^{\infty} a_j(X) \cos jn\theta + b_j(X) \sin jn\theta + a_0(X) \quad (2.1)$$

and

Since the radial deflection is an even function in θ , $b_j = 0$

$$a_j(X) = \frac{2}{Y} \int_{-\frac{Y}{2}}^{\frac{Y}{2}} \left(1 - \frac{\delta_j^0}{2} \right) w(X, \theta) \cos jn\theta d\theta \quad (2.2)$$

From symmetry

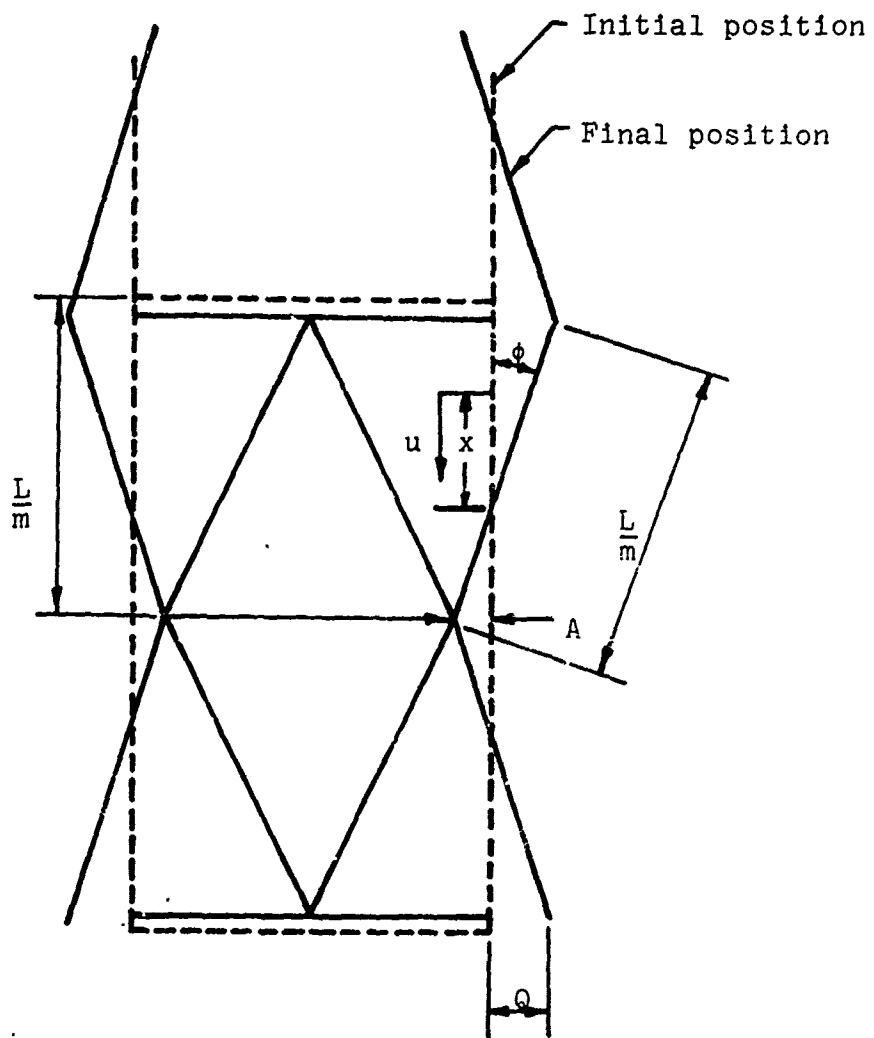


Fig. A4 Detailed Axial Section for u Displacement
Determination

$$a_j(x) = \frac{4}{Y} \int_0^{\frac{Y}{2}} (1 - \frac{1}{2} \delta_j^0) w(x, \theta) \cos jn\theta d\theta \quad (2.3)$$

$$= \frac{2n}{\pi} \left[\int_0^{\theta_p(x)} (1 - \frac{1}{2} \delta_j^0) \cos jn\theta d\theta + \int_{\theta_p(x)}^{\frac{Y}{2}} (1 - \frac{1}{2} \delta_j^0) w(x, \theta = \theta_p) \cos jn\theta d\theta \right] \quad (2.4)$$

where

$$\theta_p(x) = \frac{l_y}{a} \left[1 - \frac{x}{l_x} \right] = \frac{\pi}{n} \left[1 - \frac{mx}{L} \right] \quad (2.5)$$

Now considering the symmetry of the deformation (Fig. 4)

$$W(x) \text{ for } \theta(x) \geq \theta_p(x) = W(l_x - x) \text{ for } \theta_1(l_x - x) \leq \theta_{p1}(l_x - x) \quad (2.6)$$

And since it is also symmetrical about $x = l_x$, only $0 \leq x \leq l_x$ must be considered.

When

$$\theta(x) \begin{cases} = \theta_p(x) \\ = \frac{Y}{2} \end{cases}, \text{ then } \theta_1(l_x - x) \begin{cases} = \theta_{p1}(l_x - x) \\ = 0 \end{cases} \quad (2.7)$$

where $\theta_{p1}(l_x - x)$ is the initial position angular coordinate at $x = l_x - x$

$$\theta_{p1}(l_x - x) = \frac{l_y}{a} \left[1 - \frac{l_x - x}{l_x} \right] = \frac{l_y x}{a l_x} = \frac{m\pi x}{nL} \quad (2.8)$$

and $\theta_{p1}(l_x - x)$ is the slope discontinuity angular limit in the initial position angular coordinate at $x = l_x - x$.

To facilitate reduction of the second integral in Eq. (2.4) transform it to the variable $\theta_1(l_x - x)$.

$$\theta_1(l_x - x) = \frac{Y}{2} - \theta(x) \quad (2.9)$$

$$\theta(X) = \frac{Y}{2} - \theta_1(l_x - X) = \frac{\pi}{n} - \theta_1(l_x - X) \quad (2.10)$$

$$d\theta(X) = -d\theta_1(l_x - X)$$

Substituting Eqs. (2.6) through (2.10) into Eq. (2.4) yields

$$\begin{aligned} a_j(X) &= \frac{2n}{\pi} \left[\int_0^{\theta_p(X)} (1 - \frac{1}{2}\delta_j^\circ) w(X, \theta) \cos jn\theta d\theta \right. \\ &\quad \left. + \int_0^{\theta_{p_1}(l_x - X)} (1 - \frac{1}{2}\delta_j^\circ) w(l_x - X, \theta_1) \cos jn(\frac{Y}{2} - \theta_1)(-d\theta_1) \right] \\ a_j(X) &= \frac{2n}{\pi} (1 - \frac{1}{2}\delta_j^\circ) \left[\int_0^{\theta_p(X)} w(X, \theta) \cos jn\theta d\theta \right. \\ &\quad \left. + \int_0^{\theta_{p_1} = \frac{nY}{2L}} w(l_x - X, \theta_1) \cos jn(\frac{Y}{2} - \theta_1) d\theta_1 \right] \quad (2.11) \end{aligned}$$

Now

$$\cos jn(\frac{Y}{2} - \theta_1) = \cos jn(\frac{\pi}{n} - \theta_1) = \cos(j\pi - jn\theta_1) = (-1)^j \cos jn\theta_1 \quad (2.12)$$

and from Eq. (1.11)

$$w(l_x - X, \theta_1) = [a + c_2(l_x - X)] \cos \theta_1 + a \theta_1 \sin \theta_1 - a \quad (2.13)$$

but from Eq. (1.3)

$$c_2(l_x - X) = c_1(X) \quad 0 \leq X \leq l_x \quad (2.14)$$

Evaluating the first integral in Eq. (2.11) by use of Eqs. (1.11) yields

$$\begin{aligned} \int_0^{\theta_p(X)} w(X, \theta) \cos jn\theta d\theta &= \left\{ [a + c_2(X)] \frac{1}{2} \left[\frac{\sin E\theta}{E} + \frac{\sin F\theta}{F} \right] + \frac{a}{2} \left[\frac{\sin E\theta}{E^2} \right. \right. \\ &\quad \left. \left. + \frac{\sin F\theta}{F^2} \right] - \frac{a\theta}{2} \left[\frac{\cos E\theta}{E} + \frac{\cos F\theta}{F} \right] \right\}_{\theta=0}^{\theta=\theta_p} - \frac{a \sin jn\theta_p}{jn} \\ &= \frac{1}{2} \left\{ \frac{\sin E\theta_p}{E} [a + c_2(X) + \frac{a}{E}] + \frac{\sin F\theta_p}{F} [a + c_2(X) \right. \\ &\quad \left. + \frac{a}{F}] - a\theta_p \left[\frac{\cos E\theta_p}{E} + \frac{\cos F\theta_p}{F} \right] \right\} - \frac{a \sin jn\theta_p}{jn} \end{aligned}$$

$$E = 1 + jn \quad F = 1 - jn$$

$$\theta_2 = \pi - \theta_1$$

$$\int_0^{\theta_1} W(X, \theta) \cos jn\theta \, d\theta = \frac{(-1)^j}{2} \left([a + c_2(X)] \left\{ \sin \frac{\pi}{n} \left[\frac{\cos E\theta_1}{E} + \frac{\cos F\theta_1}{F} \right] - \cos \frac{\pi}{n} \left[\frac{\sin E\theta_1}{E} + \frac{\sin F\theta_1}{F} \right] \right\} \right. \\ \left. + 2 \left\{ \sin \frac{\pi}{n} \left[\frac{\cos E\theta_1}{E^2} + \frac{\cos F\theta_1}{F^2} \right] - \cos \frac{\pi}{n} \left[\frac{\sin E\theta_1}{E^2} + \frac{\sin F\theta_1}{F^2} \right] \right\} \right. \\ \left. - a \left(\frac{\pi}{n} - \theta_1 \right) \left\{ \sin \frac{\pi}{n} \left[\frac{\sin E\theta_1}{E} + \frac{\sin F\theta_1}{F} \right] + \cos \frac{\pi}{n} \left[\frac{\cos E\theta_1}{E} + \frac{\cos F\theta_1}{F} \right] \right\} \right) \\ - \frac{2}{jn} \left[\sin j\pi \cos jn\theta_1 - (-1)^j \sin jn\theta_1 \right] \quad (2.15)$$

Evaluating the second integral in Eq. (2.11) after substituting Eq. (2.13) and (2.14)

$$\int_0^{\theta_1} W(X - X, \theta_1) \cos jn \left(\frac{X}{2} - \theta_1 \right) d\theta_1 = (-1)^j \left([a + c_1(X)] \frac{1}{2} \left[\frac{\sin E\theta_1}{E} + \frac{\sin F\theta_1}{F} \right] + \frac{2}{2} \left\{ \left[\frac{\sin E\theta_1}{E^2} - \frac{\sin F\theta_1}{F^2} \right] \right. \right. \\ \left. \left. - \theta_1 \left[\frac{\cos E\theta_1}{E} + \frac{\cos F\theta_1}{F} \right] \right\} - \frac{2 \sin jn\theta_1}{jn} \right)_{\theta_1 = \theta_1}^{\theta_1 = \theta_1} \\ = \frac{(-1)^j}{2} \left([a + c_1(X)] \frac{1}{2} \left[\frac{\sin E\theta_1}{E} + \frac{\sin F\theta_1}{F} \right] + 2 \left\{ \frac{\sin E\theta_1}{E^2} + \frac{\sin F\theta_1}{F^2} \right\} \right. \\ \left. - \theta_1 \left[\frac{\cos E\theta_1}{E} + \frac{\cos F\theta_1}{F} \right] \right) - \frac{2 \sin jn\theta_1}{jn} \quad (2.16)$$

Adding Eqs. (2.15) and (2.16) and substituting in Eq. (2.11) yields

$$\left[\begin{aligned}
 & \frac{\sin E \theta_{\beta 1}}{E^2} \left\{ a(E+1)(1 - \cos \frac{\pi}{n}) + E \left[c_1(X) - c_2(X) \cos \frac{\pi}{n} + a(\theta_{\beta 1} - \frac{\pi}{n}) \sin \frac{\pi}{n} \right] \right\} \\
 & + \frac{\sin F \theta_{\beta 1}}{F^2} \left\{ a(F+1)(1 - \cos \frac{\pi}{n}) + F \left[c_1(X) - c_2(X) \cos \frac{\pi}{n} + a(\theta_{\beta 1} - \frac{\pi}{n}) \sin \frac{\pi}{n} \right] \right\} \\
 & + \frac{\cos E \theta_{\beta 1}}{E^2} \left\{ a[(E+1) \sin \frac{\pi}{n} - E \frac{\pi}{n} \cos \frac{\pi}{n}] + E a \theta_{\beta 1} [\cos \frac{\pi}{n} - 1] + E c_2(X) \sin \frac{\pi}{n} \right\} \\
 & + \frac{\cos F \theta_{\beta 1}}{F^2} \left\{ a[(F+1) \sin \frac{\pi}{n} - F \frac{\pi}{n} \cos \frac{\pi}{n}] + F a \theta_{\beta 1} [\cos \frac{\pi}{n} - 1] + F c_2(X) \sin \frac{\pi}{n} \right\} \\
 & - \frac{2a}{jn} (-1)^j \sin j \pi \cos j n \theta_{\beta 1}
 \end{aligned} \right] \quad (2.17)$$

$$a_j = \frac{2n(-1)^j}{2\pi} (1 - \frac{1}{2} \delta_j)$$

for $j = 0, 1, 2, \dots, J$

Eq. (2.17) reduces to

$$a_j = (1 - \frac{1}{2} \delta_j^0) \frac{a_n (-1)^j}{\pi} \left[\begin{array}{l} (1 - \cos \frac{\pi}{n}) \left(\frac{\sin E \theta_{\beta 1}}{E^2} + \frac{\sin F \theta_{\beta 1}}{F^2} \right) \\ + \sin \frac{\pi}{n} \left(\frac{\cos E \theta_{\beta 1}}{E^2} + \frac{\cos F \theta_{\beta 1}}{F^2} \right) \end{array} \right] - 2a \delta_j^0 \quad (2.18)$$

3. Determination of Fourier Coefficients for Double Fourier Series

The expression given in Eq. (2.2) used with the derived Fourier coefficient in Eq. (2.18) yields a deflection shape which has no slope discontinuities in the circumferential direction but has slope discontinuities in the axial direction. This is because $a_j(x)$ has slope discontinuities in the axial direction. In order to obtain the radial displacement function which has no axial direction slope discontinuity for a finite number of terms, the radial deflection can be expressed as a double Fourier series which is the same as expanding $a_j(x)$ in a Fourier series as a function of x or:

$$w(x, \theta) = \sum_{i=0}^{\infty} \sum_{j=0}^{\infty} a_{ij} \cos \frac{i m \pi x}{L} \cos j n \theta \quad (3.1)$$

Using $a_j(x)$ as it is defined in Eq. (2.1)

$$a_{ij} = \frac{m}{L} \int_{-\frac{L}{m}}^{\frac{L}{m}} (1 - \frac{1}{2} \delta_j^0) a_j(x) \cos \frac{i m \pi x}{L} dx \quad (3.2)$$

For a_j an even function in x

$$a_{ij} = \frac{2m}{L} \int_0^{\frac{L}{m}} [(1 - \frac{1}{2} \delta_j^0) a_j(x)] \cos \frac{i m \pi x}{L} dx \quad (3.3)$$

When Eq. (2.18) is substituted

$$a_{ij} = \frac{2amn}{\pi L} \int_0^{L/m} (1 - \frac{1}{2} \delta_j^0) (-1)^j \left[\begin{aligned} & (1 - \cos \frac{\pi}{n}) \left[\frac{\sin E \theta_{\beta 1}}{E^2} + \frac{\sin F \theta_{\beta 1}}{F^2} \right] \cos \frac{im\pi x}{L} dx \\ & + \sin \frac{\pi}{n} \left[-\frac{\cos E \theta_{\beta 1}}{E^2} + \frac{\cos F \theta_{\beta 1}}{F^2} \right] \end{aligned} \right] \quad (3.4)$$

$$- 2a \delta_j^0 \delta_i^0$$

Inspection of Eq. (3.4) indicates that there are two general types of integrals to evaluate:

$$\int_0^{L/m} \sin G \theta_{\beta 1} \cos \frac{im\pi x}{L} dx = -\frac{1}{2} \left[\frac{\cos \frac{m\pi}{L} (\frac{G}{n} + i)x}{\frac{m\pi}{L} (\frac{G}{n} + i)} + \frac{\cos \frac{m\pi}{L} (\frac{G}{n} - i)x}{\frac{m\pi}{L} (\frac{G}{n} - i)} \right]_0^{L/m}$$

$$= \frac{-GL}{mn\pi} \left[\frac{(-1)^{i+j} \cos(\frac{\pi}{n} - 1)}{[\frac{G}{n}]^2 - i^2} \right] \quad (3.5)$$

$$\text{and } \int_0^{L/m} \cos G \theta_{\beta 1} \cos \frac{im\pi x}{L} dx = \frac{GL}{mn\pi} \left[\frac{(-1)^{i+j} \sin \frac{\pi}{n}}{[\frac{G}{n}]^2 - i^2} \right] \quad (3.6)$$

since G is of the form $l \pm jn$.

Substitution of Eqs. (3.5) and (3.6) into (3.4) after simplification yields:
 For $i + j$ even

$$a_{ij} = \frac{8a}{\pi^2} \sin^2 \frac{\pi}{2n} (-1)^i \left\{ \frac{1}{E \left[\left(\frac{E}{n} \right)^2 - i^2 \right]} + \frac{1}{F \left[\left(\frac{E}{n} \right)^2 - i^2 \right]} \right\} - 2a \delta_j^0 \delta_i^0 \quad (3.7)$$

For $i + j$ odd $a_{ij} = 0$

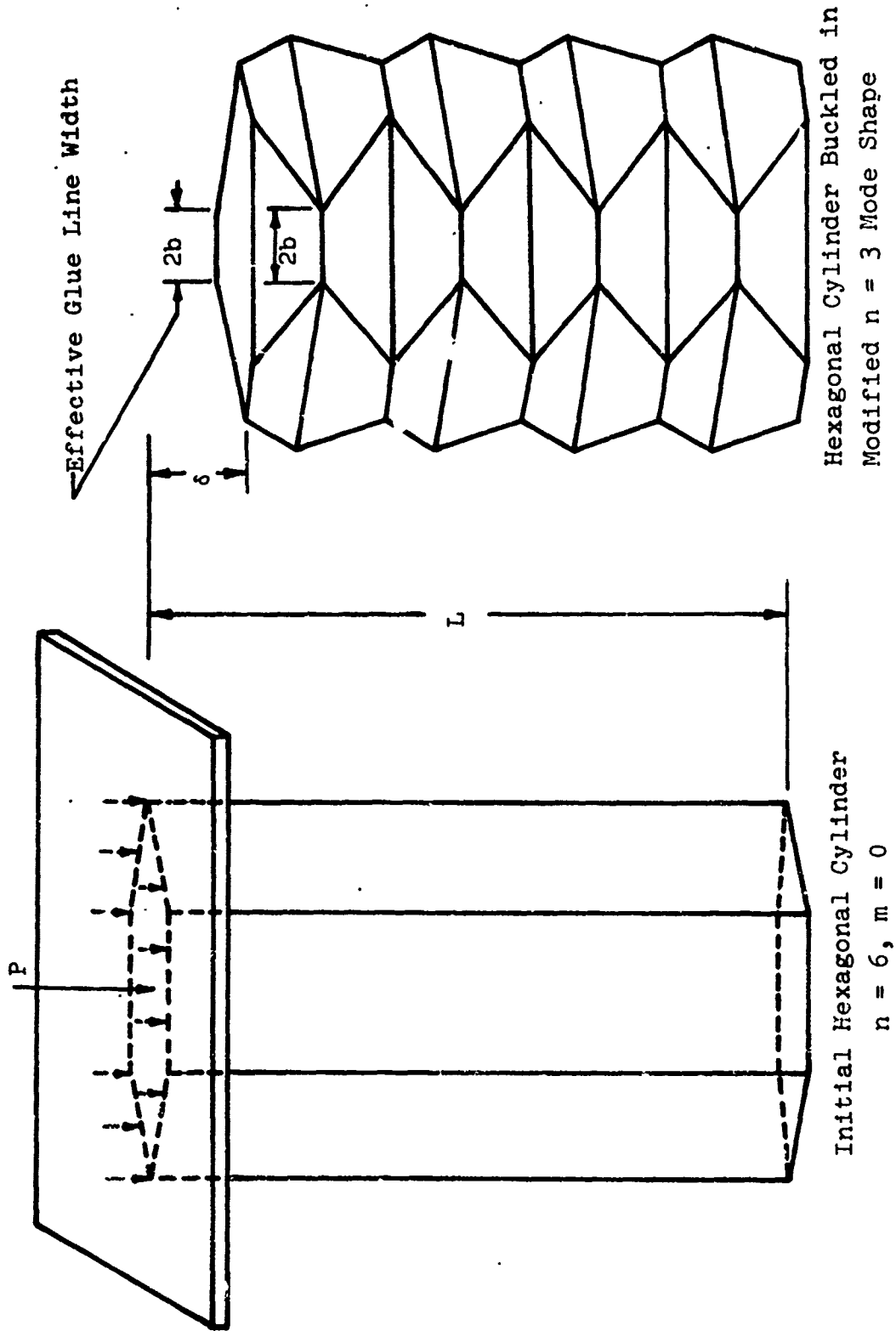
$$a_{ij} = \frac{8a}{\pi} \left(n \sin \frac{\pi}{2n} \right)^2 (-1)^i \left\{ \frac{[1 + (-1)^{i+j}] [1 + 3(jn)^2 - (in)^2]}{[1 - (jn)^2] \{ [1 - (in)^2 + (jn)^2]^2 - (2jn)^2 \}} \right\} (1 - \frac{1}{2} \delta_j^0) (1 - \frac{1}{2} \delta_i^0) - 2a \delta_j^0 \delta_i^0 \quad (3.8)$$

4. Fourier Coefficients for Honeycomb Cell

Inspection of the buckled cells of the impacted paper honeycomb specimens, Fig. 6, shows that the radial displacements from the sides which form the original hexagonal shape are alternately inward and outward as one progresses around the cell wall. The original hexagonal shape can be represented by the analytical expression for the radial displacement from the derived Eqs. (3.8) and (3.1) by using the longitudinal mode number $m = 0$ and circumferential mode number $n = 6$.

Cross sections of a buckled cylindrical shell in the $n = 3$ mode have three sides which form an equilateral triangle at the axial nodes. However, in the $n=3$ mode, there are 6 sides ($2n$) at any cross section between the axial nodes. Maximum displacements in the buckled honeycomb occur at the circumferential mid-points of the original sides of the hexagon. The difference between the maximum inward deflection at these points for the $n = 3$ mode and the $n = 6, m = 0$ mode is equal to the maximum outward deflection, Fig. 7. Thus the alternating inward and outward displacements observed in Fig. 6 are the same as the displacements of a circular cylindrical surface in a modified $n = 3$ buckling mode minus the $n = 6, m = 0$ mode which represents the original hexagonal cylindrical shape of the cell.

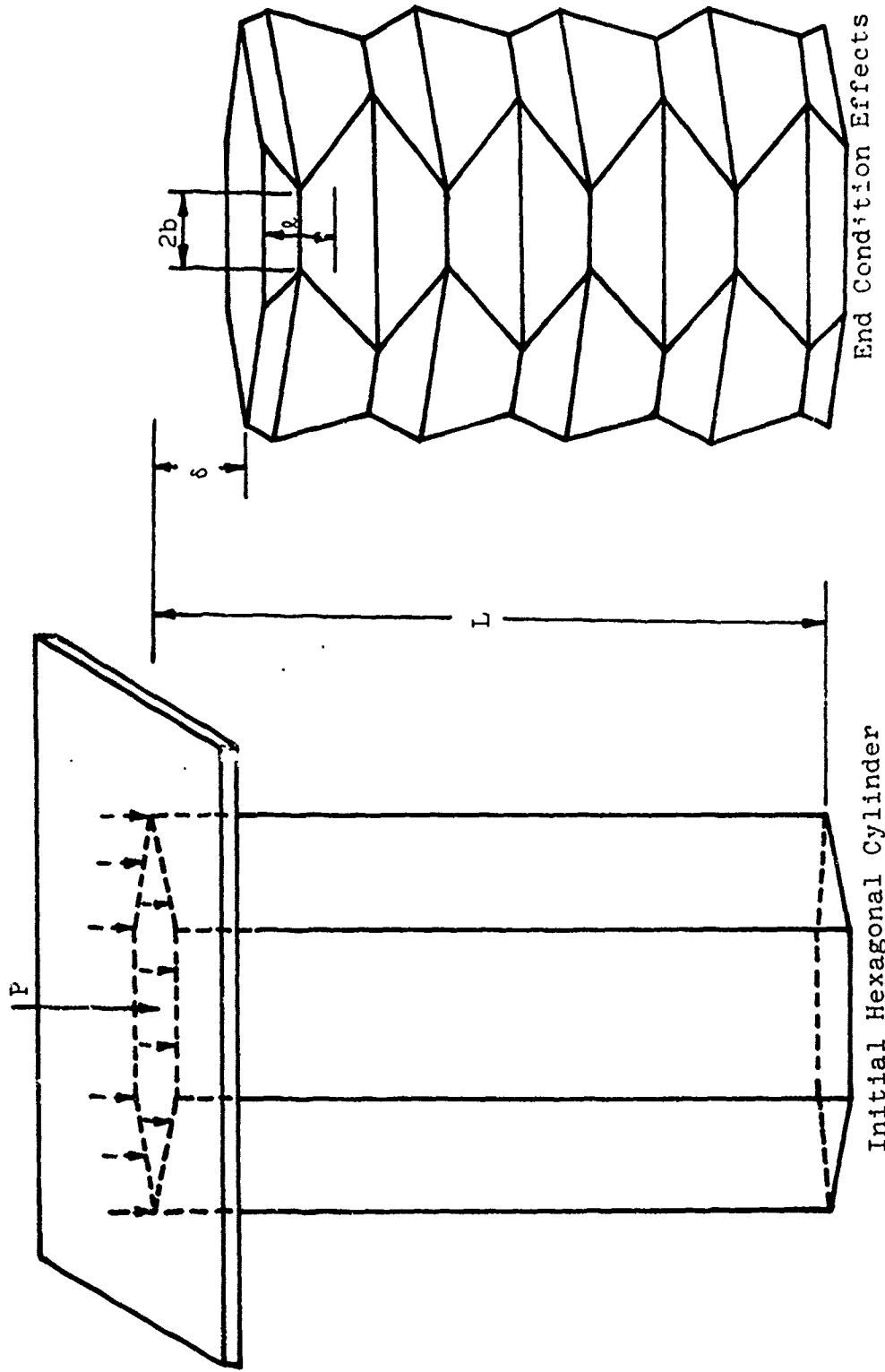
The modified $n = 3$ buckling mode of the honeycomb cells is a function of the width of the glue line which remains intact during the buckling, i.e. "the effective glue line width," see Fig. A5. Here b is the half width of the effective glue line. The cross section of a buckled circular cylindrical shell at the midpoint between the axial nodes of the $n = 3$ buckling mode is the same as the cross section for the $n = 6, m = 0$ mode. This means that the deflections are the same and consequently there is no net displacement at that section between the two deformation modes. This axial location corresponds to the end conditions of a honeycomb pad in Fig. A6 cell, where displacements are constrained by the facing paper. The radial displacements of the buckled honeycomb are determined in the following manner:



Hexagonal Cylinder Buckled in
Modified $n = 3$ Mode Shape

Initial Hexagonal Cylinder
 $n = 6, m = 0$

Fig. A5 Modified Form of $n = 3$ Mode Shape



Initial Hexagonal Cylinder
 $n = 6, m = 0$

FIG. A6 End Condition Effects on Mode Shape

Referring to Fig. 8, the radial deflection in the modified $n = 3$ shape may be expressed as:

$$\begin{aligned}
 W_{n=3 \text{ mod}}(X_1, \theta) &= \sum_{i=0}^{\infty} \sum_{j=0}^{\infty} a_{ij3} \cos 3j\theta \cos \frac{i m \pi X_1}{L(1 - \frac{6b}{\pi a})} \\
 &= \sum_{j=0}^{\infty} a_{j3}(X_1) \cos 3j\theta
 \end{aligned}
 \tag{4.1}$$

where

$$X_1 = X - \frac{3bL}{m\pi a}
 \tag{4.2}$$

and

$$a_{ij3}(X_1) = \sum_{i=0}^{\infty} a_{ij3} \cos \frac{i m \pi X_1}{L(1 - \frac{6b}{\pi a})}
 \tag{4.3}$$

$$a_{ij3} = \frac{2n}{\pi} \sum_{j=0}^{\infty} \left[\frac{(-1)^j (1 - \frac{1}{2} \delta_j)}{E^2} \right] \left[\begin{aligned} &(1 - \cos \frac{\pi}{n}) \left[\sin \frac{Em\pi}{nL} (X_1 + \frac{3bL}{m\pi a}) \right] \\ &+ \sin \frac{\pi}{n} \left[\cos \frac{Em\pi}{nL} (X_1 + \frac{3bL}{m\pi a}) \right] \end{aligned} \right] - 2\delta_j^0
 \tag{4.4}$$

+ same thing with F for E

Integrals are of the form:

$$\int_0^T \sin A(z+B) \cos \frac{i\pi z}{T} dz = \int_0^T [\sin Az \cos AB + \cos Az \sin AB] \cos \frac{i\pi z}{T} dz \quad (4.5)$$

$$\int_0^T \cos A(z+B) \cos \frac{i\pi z}{T} dz = \int_0^T [\cos Az \cos AB - \sin Az \sin AB] \cos \frac{i\pi z}{T} dz \quad (4.6)$$

where

$$A = \frac{(1 \pm jn) m \pi}{nL}$$

$$B = \frac{3bL}{\pi a m}$$

$$T = \frac{L}{m} \left(1 - \frac{6b}{\pi a}\right)$$

$$\int_0^T \sin Az \cos \frac{i\pi z}{T} dz = -\frac{1}{2} \left[\frac{\cos(A + \frac{i\pi}{T})z}{(A + \frac{i\pi}{T})} + \frac{\cos(A - \frac{i\pi}{T})z}{(A - \frac{i\pi}{T})} \right]_0^T$$

$$= -(-1)^j A \left[\frac{\cos AT - (-1)^j}{A^2 - (\frac{i\pi}{T})^2} \right] \quad (4.7)$$

$$\int_0^T \cos Az \cos \frac{i\pi z}{T} dz = (-1)^j A \left[\frac{\sin AT}{A^2 - (\frac{i\pi}{T})^2} \right] \quad (4.8)$$

Substituting these integrals into Eq. (4.4) and simplifying yields:

$$a_{ij3} = \frac{2a}{(1 - \frac{6b}{\pi a})\pi^2} \cdot \frac{(1 - \frac{1}{2}\delta_j^0)(-1)^{i+j}}{E[E^2 - \frac{1}{2}(\frac{6b}{\pi a})^2]} - a\delta_i^0\delta_j^0$$

$$+ \sin\frac{\pi}{3} [(-1)^j \cos E(\frac{b}{a} - \frac{\pi}{3}) + (-1)^i \cos \frac{Eb}{a}]$$

$$+ \sin\frac{\pi}{3} [(-1)^j \sin E(\frac{b}{a} - \frac{\pi}{3}) - (-1)^i \sin \frac{Eb}{a}]$$

+ the same thing with F for E

(4.9)

5. Strain Energy Expressions

To obtain the critical buckling stress the strain energy is calculated and then equated to the work done by the force required to cause the buckling. The strain energy calculation proceeds as follows. Transform the axial coordinate x_1 in Eq. (4.1) to a new axial coordinate x_2 (see Fig. 8). This is done in order to satisfy the natural boundary conditions of zero deflection and simple support at the limits of integration in the strain energy expression. The transformation relationships are:

$$x_2 = l_x - \frac{6bl_x}{\pi a}, \quad x_2 = 0 \quad \text{at the limits}$$

$$x_2 = x_1 - \frac{l_x}{2} + \frac{3bl_x}{\pi a} \quad \text{between the limits}$$

Insert this expression in Eqs. (3.1) and (4.1) and subtract to obtain the net radial deflection of the hexagonal cell. Note that $w(x, \epsilon)$ when $n = 6$, $m = 0$ reduces to

$$\sum_{i=0}^{\infty} \sum_{j=0}^{\infty} a_{ij6} \cos 6j\theta$$

which can be written

$$\sum_{i=0}^{\infty} \sum_{j=0}^{\infty} \frac{1 + (-1)^j}{2} a_{ij6} \cos 3j\theta$$

$$W_H = W_{3med} - W_{n=6} = \sum_{i=0}^{\infty} \sum_{j=0}^{\infty} a_{ij3} \left[a_{ij3} \cos \left\{ \frac{im\pi(x_2 + \frac{L}{2} - \frac{3bLx}{\pi a})}{L(1 - \frac{6b}{\pi a})} \right\} - \frac{(1 + (-1)^j)}{2} a_{ij\frac{6}{2}} \right] \cos 3j\theta$$

(5.1)

From Ref. 10 the bending energy U_b of the entire shell is

$$U_b = \frac{Et^3}{24(1-\nu)^2} \frac{L}{m} \frac{L(1 - \frac{6b}{\pi a})}{\pi^3} \int_0^{2\pi} \int_0^{\frac{L}{m}(1 - \frac{6b}{\pi a})} \left[W_{,xx} + \frac{W_{,\theta\theta}}{a^2} \right] - 2(1-\nu) \left[W_{,xx} \frac{W_{,x\theta}}{a^2} - \left(\frac{W_{,x\theta}}{a} \right)^2 \right] a dx d\theta$$

(5.2)

The stretching energy is

$$U_e = \frac{Et}{2(1-\nu^2)} \frac{L}{m} \frac{L(1 - \frac{6b}{\pi a})}{\pi^2} \int_0^{2\pi} \int_0^{\frac{L}{m}(1 - \frac{6b}{\pi a})} \left[(\epsilon_x + \epsilon_\theta)^2 - 2(1-\nu)(\epsilon_x \epsilon_\theta - \frac{\epsilon_{x\theta}^2}{4}) \right] a dx d\theta$$

(5.3)

For a developable surface there would be no stretching energy. However, if only a finite number of terms are included in the Fourier series expression for $w(x, \theta)$ the curvature at the folds will be finite and the surface will not be a developable surface. Hence there will be some stretching energy.

The exact large displacement strains are:

$$\epsilon_x = u_{,x} + \frac{1}{2} [u_{,x}^2 + v_{,x}^2 + w_{,x}^2] \quad (5.4)$$

$$\epsilon_\theta = \frac{v_{,0}}{a} + \frac{1}{2a^2} [u_{,0}^2 + v_{,0}^2 + w_{,0}^2] - \frac{w}{a} \quad (5.5)$$

$$\epsilon_{x\theta} = \frac{u_{,0}}{a} + v_{,x} + \frac{u_{,x} u_{,0}}{a} + \frac{v_{,x} v_{,0}}{a} + \frac{w_{,x} w_{,0}}{a} \quad (5.6)$$

Differentiating Eq. (5.1) and substituting in Eq. (5.2) yields:

$$\begin{aligned}
 U_b = & \frac{Et^3}{24(1-\nu^2)} \frac{am}{(1-\frac{6b}{\pi a})} \int_0^{\frac{L}{m}(1-\frac{6b}{\pi a})} \int_0^{2\pi} P \, dx d\theta \quad (5.7) \\
 & \left[- \frac{m^2 \pi^2}{L^2 (1-\frac{6b}{\pi a})^2} i^2 a_{ij3} \cos 3j\theta \cos \frac{im\pi}{L} \frac{x_2 + \frac{lx}{2} - \frac{36lx}{\pi a}}{L(1-\frac{6b}{\pi a})} \right. \\
 & \quad \left. - \frac{9}{a^2} j^2 \left\{ a_{ij3} \cos \frac{im\pi}{L} \frac{x_2 + \frac{lx}{2} - \frac{36lx}{\pi a}}{(1-\frac{6b}{\pi a})} - \frac{(1+(-1)^j)}{2} a_{ij6} \right\} \cos 3j\theta \right] \\
 & - 2(1-\nu) \left[\frac{9}{a^2} \frac{m^2 \pi^2}{a^2 L^2 (1-\frac{6b}{\pi a})^2} i^2 a_{ij3} \cos 3j\theta \cos \frac{im\pi}{L} \frac{x_2 + \frac{lx}{2} - \frac{36lx}{\pi a}}{L(1-\frac{6b}{\pi a})} \right. \\
 & \quad \left. \left[j^2 \left\{ a_{ij3} \cos \frac{im\pi}{L} \frac{x_2 + \frac{lx}{2} - \frac{36lx}{\pi a}}{(1-\frac{6b}{\pi a})} - \frac{[1+(-1)^j]}{2} a_{ij6} \right\} \cos 3j\theta \right] \right] \\
 & + 2 \frac{(1-\nu)}{a^2} \left[3 \frac{m\pi}{L(1-\frac{6b}{\pi a})} ij a_{ij3} \sin \frac{im\pi}{L} \frac{x_2 + \frac{lx}{2} - \frac{36lx}{\pi a}}{L(1-\frac{6b}{\pi a})} \sin 3j\theta \right]^2
 \end{aligned}$$

$$P = \sum_i \sum_j$$

This document is copyrighted by the American Institute of Physics (AIP) Publishing Company. This article is intended solely for the personal use of the individual user and is not to be disseminated broadly.

The integrals in Eq. (5.7) are orthogonal. Integrating and collecting terms yields:

$$\begin{aligned}
 U_6 &= \frac{E t^3 \pi L a}{48 (1-\nu^2)} \sum_{i=0}^4 \sum_{j=0}^Q Q \\
 &\left\{ \begin{aligned}
 & \left[\frac{m\pi}{L(1-\frac{6b}{\pi a})} \right]^4 i^4 a_{ij3}^2 - (2-\nu) \frac{18}{a^2} i^2 j^2 [a_{ij3}^2 - [1+(-1)^j] \delta_i^0 a_{ij3} a_{ij6} \frac{1}{2} \left[\frac{m\pi}{L(1-\frac{6b}{\pi a})} \right]^2] \\
 & + \frac{81}{a^4} j^4 [a_{ij3}^2 - 2a_{ij3} a_{ij6} \frac{1}{2} \delta_i^0 + \frac{1}{2} [1+(-1)^j] a_{ij6}^2] \\
 & + 2 \frac{(1-\nu)}{a^2} \left[9 \frac{m^2 \pi^2}{L^2 (1-\frac{6b}{\pi a})} i^2 j^2 a_{ij3}^2 \right]
 \end{aligned} \right\} \quad (5.8)
 \end{aligned}$$

Since the deformation is axially symmetric

$$u \neq f(\theta) \quad \text{and} \quad u_{,\theta} = 0$$

This reduces Eq. (5.5) and (5.6) to

$$\begin{aligned}
 \xi_X &= u_{,X} + \frac{u_{,X}^2}{2} + \frac{v_{,X}^2}{2} + \frac{w_{,X}^2}{2} \\
 \xi_\theta &= \frac{v_{,\theta}}{2} + \frac{v_{,\theta}^2}{2a^2} + \frac{w_{,\theta}^2}{2a^2} - \frac{w}{a} \\
 \xi_{X\theta} &= v_{,X} + v_{,X} \frac{v_{,\theta}}{a} + w_{,X} \frac{w_{,\theta}}{a}
 \end{aligned}
 \tag{5.9}$$

From Eq. (5.1) $w = w_{3\text{mod}} - w_{n=6}$ and Eqs. (1.15) and (1.16) yield

$$v = + \int w d\theta$$

$$v_{,\theta} = w$$

$$v_{,X} = \int w_{,X} d\theta$$

(5.10)

Substituting from Eq. (5.10) in (5.9) and assuming

$$\begin{aligned}
 \xi_X &= u_{,X} + \frac{u_{,X}^2}{2} + \frac{1}{2} \left[\int w_{,X} d\theta \right]^2 + \frac{w_{,X}^2}{2} \\
 \xi_\theta &= \frac{1}{2a^2} \left\{ w^2 + \frac{w_{,\theta}^2}{2a^2} \right\} \\
 \xi_{X\theta} &= \int w_{,X} d\theta + \frac{w}{a} \int w_{,X} d\theta + \frac{w_{,X} w_{,\theta}}{a}
 \end{aligned}
 \tag{5.11}$$

Substituting these expressions in Eq. (5.3) yields:

$$U_e = \frac{E t a}{2(1-\nu^2)} \int \int \left\{ \begin{aligned} & u_{yx}^2 + u_{yx}^3 + u_{yx} [\int w_{yx} d\theta]^2 + u_{yx} w_{yx}^2 + \frac{u_{yx}^4}{4} + \frac{u_{yx}^2}{2} [\int w_{yx} d\theta]^2 + \frac{u_{yx} w_{yx}^2}{2} \\ & + \frac{1}{4} [\int w_{yx} d\theta]^4 + \frac{1}{2} [\int w_{yx} d\theta]^2 w_{yx}^2 + \frac{w_{yx}^4}{4} + \frac{1}{4a} [w_{yx}^2 w_{y0}^2 + w_{y0}^4] \\ & + \frac{\nu}{a^2} [u_{yx} (w^2 + w_{y0}^2) + \frac{u_{yx}^2}{2} (w^2 + w_{y0}^2)] + \frac{1}{2} [w^2 + w_{y0}^2] [\int w_{yx} d\theta]^2 + w_{yx}^2 \\ & + \frac{(1-\nu)}{2} \left\{ \left[\int w_{yx} d\theta \right]^2 \left(1 + \frac{w}{a} \right)^2 + 2 \int w_{yx} d\theta \left[1 + \frac{w}{a} \right] \frac{w_{yx} w_{y0}}{a} + \left[\frac{w_{yx} w_{y0}}{a} \right]^2 \right\} \end{aligned} \right\} \quad (5.12)$$

From Eq. (5.1)

$$\begin{aligned} [\int w_{yx} d\theta]^2 &= \left\{ \int \left[-\frac{m\pi}{L(1-\frac{6b}{\pi a})} \sum_{i=0}^{\infty} \sum_{j=0}^{\infty} a_{ij3} \sin \frac{im\pi x}{L(1-\frac{6b}{\pi a})} \cos 3j\theta d\theta \right]^2 \right. \\ &= \frac{m^2 \pi^2}{9L^2(1-\frac{6b}{\pi a})^2} \left[\sum_{i=0}^{\infty} \sum_{j=0}^{\infty} \frac{1}{j} a_{ij3} \sin \frac{im\pi x}{L(1-\frac{6b}{\pi a})} \sin 3j\theta \right]^2 \end{aligned} \quad (5.13)$$

Neglecting third and higher powers of derivatives except in u_1 produces

$$U_e = \frac{Eh}{2(1-\nu^2)} \iint \left\{ \begin{aligned} & u_{1,x} \left\{ u_{1,x} + u_{2,x}^2 + w_{2,x}^2 + \frac{u_{2,x}^3}{4} + [w_{2,x}] + \frac{u_{2,x}}{2} + \left[\frac{u_{2,x}}{2} + \frac{u_{2,x}}{2} \right] + \frac{u_{2,x} w_{2,x}^2}{2} \right\} \\ & + \nu \frac{u_{2,x}}{a^2} \left\{ [w^2 + w_{2,\theta}^2] \left[1 + \frac{u_{2,x}}{2} \right] + (1-\nu) \left[\int w_{2,x} d\theta \right]^2 \right\} \end{aligned} \right\} a dx d\theta \quad (5.14)$$

$u(x)$ is axial displacement function
 $u(0) = 0$, the total displacement = $u(L)$
For one buckling length u is defined in Eq. (1.20).

$$\epsilon_{tot} = \frac{m}{L(1 - \frac{6b}{\pi a})} u \left(x = \frac{L}{m} \left(1 - \frac{6b}{\pi a} \right) \right) \quad (5.15)$$

$$P_{cr} = \frac{U_b + U_e}{\epsilon_{tot}} \quad (5.16)$$

From Eq. (1.18) it can be seen that u is a function of $\sin \phi$ which can be determined in the following manner:

$$\sin \phi = \frac{|[W_{max}] - [W_{min}]|}{\rho} = \frac{|[W_{x=0}]_{\theta=0} - [W_{x=\rho_x}]_{\theta=0}|}{\rho} \quad (5.17)$$

For the modified $n = 3$ deflection shape, w is minimum at $x = 0$, and maximum at $x = \rho_x (1 - \frac{6b}{\pi a})$.

From Eq. (5.1)

$$w_{ij} = \sum_i \sum_j \left\{ a_{ij3} \cos \frac{im\pi x}{L(1-\frac{6b}{\pi a})} - \frac{(1+(-1)^j)}{2} a_{ij6} \right\} \cos 3j\theta \quad (5.18)$$

$$w_{ijmin} = \sum_j \left\{ a_{ij3} - \frac{(1+(-1)^j)}{2} a_{ij6} \right\}$$

$$w_{ijmax} = \sum_j \left\{ a_{ij3} \cos i\pi - \frac{(1+(-1)^j)}{2} a_{ij6} \right\}$$

$$\sin \phi_{ij} \cong \sum_j \left| \frac{a_{ij3}(1 - \cos i\pi)}{\frac{L}{m} (1 - \frac{6b}{\pi a})} \right| \quad (5.19)$$